ACS OMEGA

http://pubs.acs.org/journal/acsodf

Article

Understanding the Mannose Transfer Mechanism of Mycobacterial Phosphatidyl-myo-inositol Mannosyltransferase A from Molecular Dynamics Simulations

Gourab Bhattacharje, Amit Ghosh,* and Amit Kumar Das*

Cite This: *ACS Omega* 2022, 7, 19288−19304

Read Online

ACCESS | Metrics & More | Article Recommendations | Supporting Information

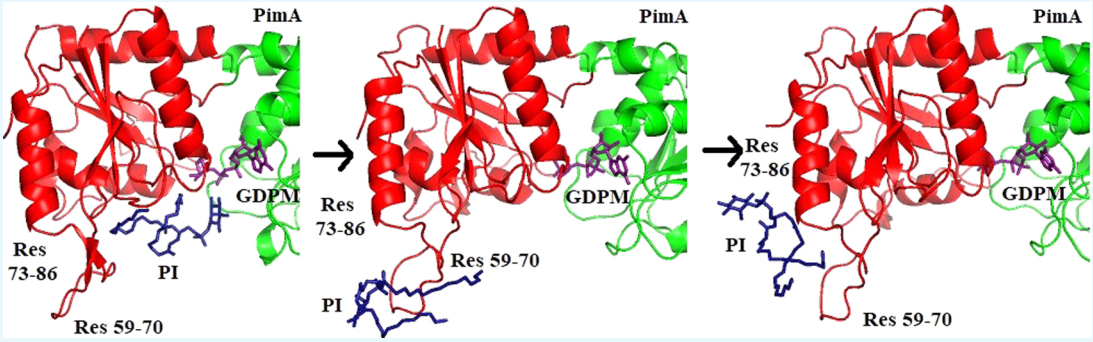

ABSTRACT: Glycolipids like phosphatidylinositol hexamannosides (PIM_6) and lipoglycans, such as lipomannan (LM) and lipoarabinomannan (LAM), play crucial roles in virulence, survival, and antibiotic resistance of various mycobacterial species. Phosphatidyl-myo-inositol mannosyltransferase A (PimA) catalyzes the transfer of the mannose moiety (M) from GDP-mannose (GDPM) to phosphatidyl-myo-inositol (PI) to synthesize GDP and phosphatidyl-myo-inositol monomannoside (PIM). This PIM is mannosylated, acylated, and further modified to give rise to the higher PIMs, LM, and LAM. It is yet to be known how PI, PIM, PI-GDPM, and PIM-GDP interact with PimA. Here, we report the docked structures of PI and PIM to understand how the substrates and the products interact with PimA. Using molecular dynamics (MD) simulations for 300 ns, we have investigated how various ligand-bound conformations change the dynamics of PimA. Our studies demonstrated the "open to closed" motions of PimA. We observed that PimA is least dynamic when bound to both GDPM and PI. MD simulations indicated that the loop residues 59−70 and the α-helical residues 73−86 of PimA play important roles while interacting with both PI and PIM. MD analyses also suggested that the residues Y9, P59, R68, L69, N97, R196, R201, K202, and R228 of PimA play significant roles in the mannose transfer reaction. Overall, docking studies and MD simulations provide crucial insights to design future therapeutic drugs against mycobacterial PimA.

1. INTRODUCTION

All bacteria from the Mycobacterium genus employ a complex cell envelope that is crucial for their virulence, survival, and antibiotic resistance.[1] Phosphatidyl-myo-inositol mannosides (PIMs) are unique glycolipids that are abundantly found at the plasma membrane of the cell envelopes of mycobacterial species and a few other actinomycetes.[2−4] These PIMs are formed on the lipid base of phosphatidyl-myo-inositol (PI), a regular content of the cell membrane of many eukaryotes and prokaryotes. Phosphatidyl-myo-inositol mannosyltransferase A (PimA) catalyzes the transfer of the mannose sugar (M) from GDP-mannose (GDPM) to the 2-position of the inositol moiety of PI (Figure 1A) in the cytosolic side of the plasma membrane to help the formation of PIM and leave GDP as a byproduct.[5,6] This PIM compound is then taken up by another enzyme, phosphatidyl-myo-inositol mannosyltransferase B′ (PimB′), and one more mannose sugar (M) is added to the 6-position of the inositol moiety of PIM (Figure 1B) to form phosphatidylinositol dimannoside, PIM_2.[7] Phosphatidylinositol mannoside acyltransferase A (PatA) can add an acyl group to the 6-position of the mannose ring attached at the 2-position of the myo-inositol of PIM_2 to produce Ac_1PIM_2.[8] An unknown acyltransferase can add another acyl group at the 3-position of the inositol group of Ac_1PIM_2 to synthesize Ac_2PIM_2.[9] In one of the strains of *Mycobacterium tuberculosis*, PimC had been identified that can add another mannose to the Ac_1PIM_2 to produce Ac_1PIM_3.[10] A previous study had

Received: February 10, 2022
Accepted: May 20, 2022
Published: June 1, 2022

ACS Publications

© 2022 The Authors. Published by American Chemical Society

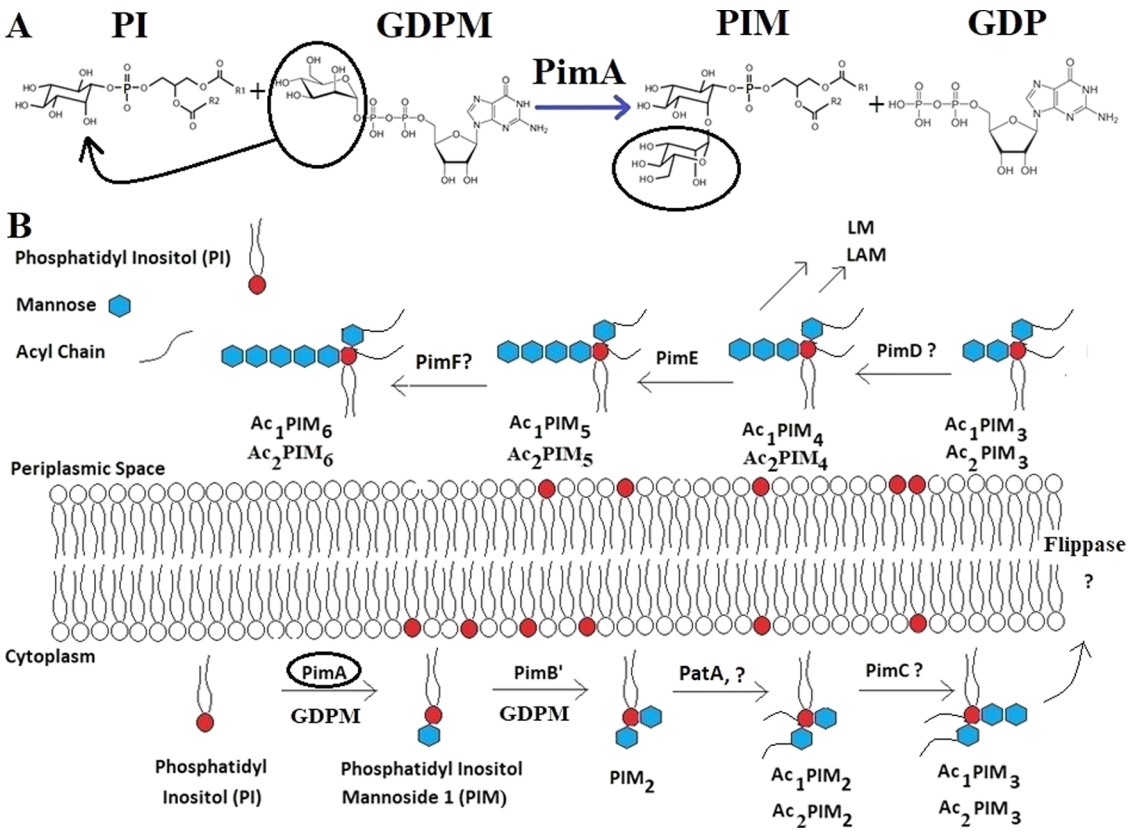

Figure 1. Role of PimA in PIM_6/LipoMannan (LM)/LipoArabinoMannan (LAM) biosynthesis of mycobacteria. (A). PimA helps transfer the mannose group of GDP-mannose (GDPM) to phosphatidyl-myo-inositol (PI) for the synthesis of PIM ($\alpha(1 \rightarrow 2)$ glycosidic linkage). Adapted with permission from Rodrigo-Unzueta et al., 2016.[19] Copyright [2016] [Elsevier]. (B). Synthesis of PIM by PimA is followed by mannosylation and acylation to produce Ac_1PIM_3/Ac_2PIM_3. Further, Ac_1PIM_3/Ac_2PIM_3 is then probably transported to the periplasmic space by an unknown flippase to further synthesize LM, LAM, and PIM_6.

suggested that the conversion from Ac_1PIM_3 to Ac_1PIM_4 may occur at the periplasmic side of the inner membrane.[11] This indicates that Ac_1PIM_3/Ac_2PIM_3 is probably the intermediate that is translocated from the cytoplasmic side to the periplasmic side by an unknown flippase. PimD, which can potentially add another mannose sugar to Ac_1PIM_3/Ac_2PIM_3 to synthesize Ac_1PIM_4/Ac_2PIM_4, is yet to be identified. This $Ac_{1/2}PIM_4$ is then either converted to $Ac_{1/2}PIM_6$ by PimE[12] and another unknown enzyme or used to synthesize more complex lipoglycans, such as Lipomannan (LM) and Lipoarabinomannan (LAM).[9,13] Together, these PIMs, LM, and LAM are not only important for the structural integrity of the mycobacterial cell envelope, but they also play critical roles in modulating host−pathogen interactions.[13,14] The biosynthetic pathway of PIMs, LM, and LAM may become novel drug targets to cure various mycobacterial diseases.

It had been previously shown *in vivo* that PimA is essential for the growth and survival of*Mycobacterium smegmatis*[5] and *Mycobacterium tuberculosis*.[15] To explore one of the first steps toward the synthesis of these complex lipoglycans, understanding the mechanism of mannose transfer by PimA is very important. Besides, PimA, a member of the glycosyltransferase family 4 (GT4) of retaining glycosyltransferases (CAZy: carbohydrate active enzyme database), helps retain the stereochemical configuration on the anomeric carbon of the mannose added to PI.[16,17] However, the mechanism behind this retention of configuration remains mostly unknown. The atomic-level structures of PimA from*M. smegmatis* had previously been elucidated in its free form or GDPM- and GDP-bound conformations using X-ray crystallography.[6,18] Similar to many nucleotide-binding proteins, PimA adopts a typical GT-B fold of glycosyltransferases and thus consists of two Rossman fold-like domains, where residues 1−169 and 170−348 form the N- and C-terminal domains, respectively.[6] The C-terminal residues 349−373 of PimA fold over to the N-terminal domain.[6] Coordinating motions of these Rossman fold-like domains gave rise to one closed conformation and another open conformation, as revealed by small-angle X-ray scattering (SAXS) studies.[20] The structure of PimA was also shown to go through secondary structure transitions while shuffling between closed and open conformations.[18] It had also been shown that the presence of both the fatty acyl chains of PI is absolutely necessary for PimA to transfer the mannose group from GDPM to PI.[6] However, how PI and PIM interact with PimA is still not clear. The open and closed conformations of PimA had been demonstrated in the presence or absence of GDP or GDPM, but detailed structural and dynamic analyses of these conformations are still lacking. Therefore, investigating the dynamics of PimA in substrate/product-bound conformations may reveal crucial steps of the mannose transfer mechanism. Moreover, how two substrates, *i.e.*, GDPM and PI, or two products, *i.e.*, GDP and PIM, interact simultaneously with PimA mostly remains unknown.

In this work, we used molecular docking analyses to find interacting residues of PimA with both PI and PIM. We have performed molecular dynamics (MD) simulations with PimA,

https://doi.org/10.1021/acsomega.2c00832
ACS Omega 2022, 7, 19288−19304

and PimA bound with PI, PIM, GDP, and GDPM, obtained from docking and previous crystallographic studies. We have also carried out MD simulations to understand how PimA interacts with both the substrates (PI and GDPM) and both the products (PIM and GDP). MD simulation trajectories were further analyzed by molecular mechanics generalized Born surface area (MMGBSA) analyses to understand the relative binding energies of PimA with each of the substrates and the products. These MD simulation analyses indicate that GDP and GDPM form relatively stable complexes with PimA, than PI and PIM, which move away from the docked-site during the simulation. The residues 59−70 and 73−86 of PimA may play crucial roles in binding both PI and PIM and thus in the mannosyl transfer mechanism. Using these analyses and previous experimental data, a hypothetical model of mannose transfer reaction by PimA has been proposed.

2. METHODS

2.1. Multiple Sequence Alignment. Protein sequences of Phosphatidyl-myo-inositol mannosyltransferases A and B′ (PimA and PimB′) of various bacteria were obtained from the uniport database.[21] Clustal Omega webserver was used to align the protein sequences.[22] Coordinates of the protein PimA of *M. smegmatis*[6,17] were downloaded from the Protein Data Bank (www.rcsb.org).[23] Sequence similarities and secondary structure information among various PimA proteins were visualized using the webserver ESPript 3.0.[24]

2.2. Molecular Docking and Preparation of the Protein−Ligand Structures. The ligand structures of phosphatidylinositol (PI) and phosphatidylinositol dimannoside (PIM_2) were obtained from the PDB entries3QI9[25] and 2GAZ,[26] respectively. PIM structure was obtained by deleting one mannose residue from PIM_2. Hydrogens were added to PI and PIM structures at pH 7.5 using the Avogadro software.[27] Both PI and PIM structures were then energy-minimized using the prodrg webserver.[28] PimA side chains were protonated at pH 7.5 using PROPKA3 webserver.[29] Molecular docking analyses were performed in the swissdock webserver (http://www.swissdock.ch/docking#).[30] Accurate and blind docking was used, where all rotatable single bonds were allowed to rotate. Flexible side chains were allowed. Results obtained from the swissdock webserver were analyzed in the Chimera program.[31] The docked structures of PimA with PI and PIM with the lowest ΔG values from a highly populated cluster were chosen to study further.

2.3. Molecular Dynamics (MD) Simulation. Molecular dynamics (MD) simulations were carried out using Gromacs 2020.3.[32] CHARMM-36 all-atom force field and TIP3P water model were used for all of the simulations. Coordinates of the GDP-bound PimA structure and PimA structure were obtained from the Protein Data Bank (PDB) file4N9W.[18] Coordinates of the ligand GDPM were obtained from the PDB file2GEJ,[6] and these coordinates were used to obtain the starting structure of the GDPM-bound PimA. Missing coordinates of the residues were reconstructed using SWISS-Model interactive webserver (http://swissmodel.expasy.org/interactive).[33] H-atoms were added to the ligand structures using the Avogadro program.[27] Ligand parameters were generated using the CHARMM General Force Field (CGenFF),[34] and the parameter files are provided in a supplementary zipped file. A rectangular box was used as a unit cell for periodic boundary conditions with a minimum distance of 10 Å from the protein PimA or any bound ligands (Table S1). Negative charges of PimA were countered by adding Na^+ atoms and Cl^- atoms in the system. Packmol package[35] was used to calculate the dimension of the rectangular box used for simulation and the number of ions required to maintain a neutralized solution with a physiological NaCl concentration of 0.16 M. Steepest descent algorithm[36] was used for energy minimizations with maximum force F_{max} not exceeding 1000 kJ mol^{-1} nm^{-1}. The system was equilibrated at a temperature of 300 K and a pressure of 1 bar by two consecutive 100 ps simulations with canonical NVT ensembles and isobaric NPT ensembles, respectively. Protein PimA and the ligands were coupled together for position restraint and thermostat coupling. Productions runs were of 300 ns each with 2 fs time steps used with Particle Mesh Ewald method for electrostatics calculations. Trajectories generated from the MD simulations were analyzed using Gromacs tools. The snapshots were visualized using the Pymol program.[37]

2.4. Principal Component Analysis (PCA). Principal component analysis (PCA) is a statistical technique that reduces the complexity of the dynamics data, and is often used to extract the collective and correlated motions of the atoms of the biological macromolecules. PCA was carried out on snapshots stored every 10 ps of the 300 ns MD simulations. Covariance matrices of C_α atoms (1119 × 1119) were constructed to capture the essential collective motions of PimA with and without ligands. A positive sign of the entries in the covariance matrix signified correlated motion, whereas a negative sign indicated anticorrelated motion between two C_α atoms. Covariance matrices were then diagonalized to produce a set of eigenvectors with respective eigenvalues. The eigenvalues represented the relevance of their corresponding eigenvectors in the system dynamics, where the eigenvectors with the largest eigenvalues signified the most relevant motions. Principal components (PCs) PC1 and PC2 were obtained by taking the projection of the displacement of the C_α atoms at each time point onto the eigenvectors 1 and 2, respectively. Gromacs tools "gmx covar" and "gmx anaeig"[32] were used to generate the covariance matrices, eigenvectors, and two-dimensional plots of PC1 versus PC2.

2.5. MMGBSA Analyses. Using the molecular mechanics generalized Born surface area (MMGBSA) approach,[38] the free energy of binding, *i.e.*, ΔG_{bind}, of a ligand (L) binding to a protein (P) to form the protein−ligand (PL) can be estimated using the following equation

$$\Delta G_{bind} = \Delta G_{PL} - \Delta G_P - \Delta G_L \quad (1)$$

Each free energy term can be decomposed into three parts: a. gas-phase molecular mechanics (MM) energy (ΔE_{MM}), b. solvation free energy (ΔG_{sol}), and c. contribution of conformational entropy ($T\Delta S$).[38]

$$\Delta G = \Delta H - T\Delta S = \Delta E_{MM} + \Delta G_{sol} - T\Delta S \quad (2)$$

ΔE_{MM} can be further decomposed into three parts: a. internal energies (ΔE_{int}), b. electrostatic energies (ΔE_{ele}), and c. van der Waals energies (ΔE_{vdW}). However, the contribution of internal energies, *i.e.*, bond, angle, and dihedral energies, toward ΔG_{bind} remains zero as no bond breaking or bond formation has been considered in this study.

$$\Delta E_{MM} = \Delta E_{int} + \Delta E_{ele} + \Delta E_{vdW} \quad (3)$$

Solvation energy can be further divided into two parts: a. electrostatic solvation energy (ΔG_{GB}) and b. nonpolar solvation energy (ΔG_{SA})[38]

https://doi.org/10.1021/acsomega.2c00832
ACS Omega 2022, 7, 19288−19304

$$\Delta G_{sol} = \Delta G_{GB} + \Delta G_{SA} \quad (4)$$

ΔG_{GB} is calculated using the generalized Born (GB) model, whereas ΔG_{SA} is estimated using solvent-accessible surface area (SASA).

$$\Delta G_{SA} = \gamma^{*}\text{SASA} + b \quad (5)$$

gmx_MMPBSA tool[38,39] was used to calculate the snapshots taken at each ns from 0 to 300 ns using igb = 2 and saltcon = 0.16.

3. RESULTS AND DISCUSSION

First, multiple sequence alignment of PimA and PimB′ was used to find the critical residues of PimA involved in the mannosyl transfer reaction (Section 3.1). PimA was then docked with both PI and PIM, and the residues important for binding were identified (Section 3.2). PimA and various ligand-bound structures of PimA were subsequently subjected to 300 ns MD simulations (Section 3.3). Backbone dynamics and compactness (Section 3.3.1), overall flexibility (Section 3.3.2), mobility of individual residues (Section 3.3.3), relative binding energies using MMGBSA analyses (Section 3.3.4), number of H-bonds formed with ligands (Section 3.3.5), secondary structure transitions (Section 3.3.6), and snapshot-analyses of various trajectories (Section 3.3.7) of PimA are discussed further, and a hypothetical scheme of mannose transfer by PimA has been proposed using the findings of this study at the end (Section 3.3.7.5).

3.1. Multiple Sequence Alignment and Identification of Critical Residues. PimA and PimB′ both incorporate GDPM as the mannose donor and act as enzymes to add mannose on PI and PIM, respectively. Resemblances in mannose donor and overall function led to analyzing the similarities in their overall sequences. Multiple sequence alignment (MSA) was attempted on the PimA and PimB′ sequences of various mycobacterial species and a related cornybacteirum species (Figure S1). MSA analysis reveals that the amino acid sequence of PimA varies a little and all of the critical residues of PimA[40] are conserved in different mycobacterial species, such as *M. tuberculosis* (H37Rv and CDC1551), *M. smegmatis*, *M. bovis*, and *M. leprae*. The crystal structures of PimA with GDP and GDPM[6] indicated that the residues G16, R196, and K202 participate in binding the β-$PO4^{2-}$, the residues G15, L194, K256, I278, V279, and E282 interact with the ribose ring, the residues P14, L194, V226, V251, D252, and D253 participate in binding the guanine ring, and the residues E274, S275, F276, and I278 bind the mannose moiety of GDPM (Figure 2A). Among these residues, G15, G16, K202, V226, E274, I278, V279, and E282 are also conserved in both PimA and PimB′.[6] Previous mutational analyses indicated that the residues Y9, Q18, Y62, N63, R68, H118, R196, E199, R201, and E274 of PimA are absolutely critical for the mannose transfer activity of PimA.[40] Among these critical residues, R196 and E274 are involved in binding GDPM. Based on the structural classification of PimA in the GT-B group of enzymes, N-terminal residues (1−169 and 349−373) were predicted to interact with the substrate PI.[41] Therefore, the residues Y9, Q18 (conserved in both PimA and PimB′), Y62, N63, R68, and H118 (conserved in both PimA and PimB′) may play important roles in binding PI or transferring of the mannose group from GDPM to PI. The residues E199 and R201, residing in the catalytic cleft (Figure 2A), may also play significant roles in the mannosyltransferase activity of PimA. The residue R201, absolutely critical for the mannosyltransferase activity of PimA, is located near R196 (absolutely critical for PimA activity and binds GDPM), E199 (absolutely critical for PimA activity), K202 (conserved in both PimA and PimB′ and binds GDPM), and situated in a highly conserved loop residues ^{200}PRKG^{203} (conserved in both

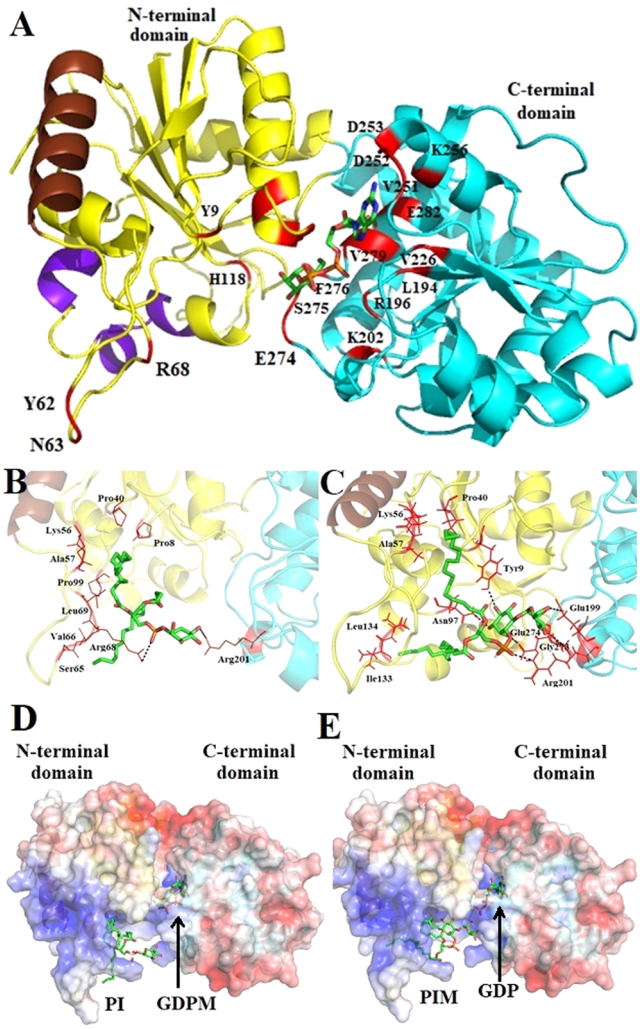

Figure 2. Residue-specific binding of PimA with GDPM, PI, and PIM as obtained from the crystal structure and molecular docking. (A). Critical residues (in red) for the mannosyl transfer reaction and GDPM binding, membrane-associated amphipathic α-helix (the residues 73−86, in chocolate), and transition of secondary structure (residues 124−131 and 134−138, in purple) are shown. The coordinates of PimA were obtained from the PDB entry4N9W.[18] (B). R68 and R201 interact with the phosphate group and the polar inositol group of PI, respectively, and the residues stabilizing the acyl groups of PI are also shown. (C). R201 interacts with the phosphate group; E199, G273, and E274 interact with the mannose group; and Y9 and N97 stabilized the inositol group of PIM; the residues interacting with the acyl chains of PIM are also shown. (D). PI (obtained from the energetically most favorable docked structure) and GDPM (obtained from the crystal structure) interacting with PimA are shown. (E). PIM (obtained from the energetically most favorable docked structure) and GDP (obtained from the crystal structure) interacting with PimA are shown. For (D) and (E), PimA surface is colored according to electrostatic charges: negatively charged, hydrophobic, and positively charged surfaces are shown in red, white, and blue colors, respectively.

https://doi.org/10.1021/acsomega.2c00832
ACS Omega 2022, 7, 19288−19304

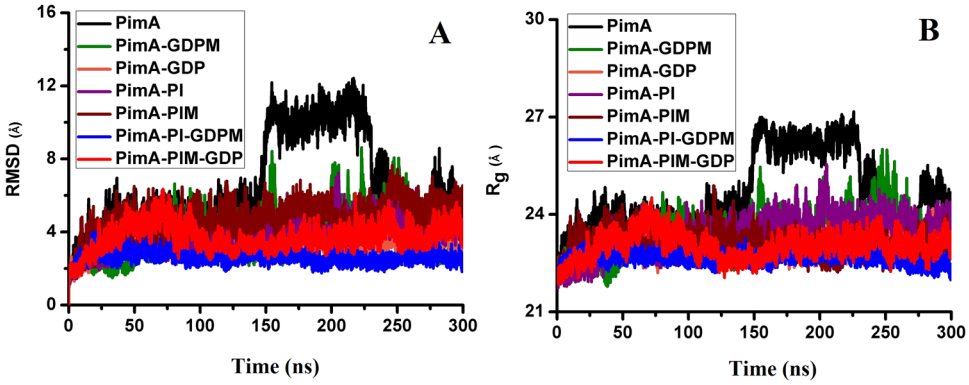

Figure 3. RMSD and R_g analyses of PimA and ligand-bound PimA. (A). RMSD values of the backbone atoms. (B) R_g values. Both (A) and (B) show a stretch of elevated values, demonstrating both "open" and "closed" conformations of PimA.

PimA and PimB′: Figure S1), and thus, is expected to play an important role for the mannosyltransferase activity of PimA.

3.2. Molecular Docking. Molecular docking of PI and PIM on PimA was attempted using the Swissdock webserver.[30] The lowest ΔG_{bind} values of PI- and PIM-docked PimA were −10.12 and −12.27 kcal/mol, which indicate that binding of both PI and PIM with PimA is energetically favorable. The docked complexes of PI-PimA and PIM-PimA are shown in Figure 2B,C, respectively. As was predicted for a GT-B enzyme,[41] the most favorable ΔG_{bind} of PI was found at the slightly positively charged N-terminal of PimA (Figure 2D). The product PIM also binds PimA at this positively charged N-terminal (Figure 2E). The presence of an extra mannose moiety along with PI involves more favorable polar interactions with PimA, which explains why the binding of PIM is energetically more favorable than that of PI. It can be observed that the O3 atom of the inositol moiety of PI interacts with the positively charged side chain of R201 (Figures 2B and S2). The residue R201, a part of the conserved residues ^{200}PRKG^{203}, binds to PI, which again indicates that the residues R196 (binds to GDPM), E199, R201, and K202 (binds to GDPM) may be involved in the addition of mannose moiety of GDPM to the O2 position of PI.[6] Docked structure of PI also showed that the residue R68 of PimA may be involved in stabilizing the phosphate group of PI by electrostatic interaction. A previous experimental study showed that mutation R68A abolished the mannosyltransferase activity of PimA.[40] One acyl chain of PI was stabilized by the interactions with the residues P8, P40, K56, A57, and P99 of PimA. The other acyl chain of PI was shown to interact with the residues S65, V66, R68, and L69, explaining a previous experimental observation where deletion of the loop residues ^{59}PIPYNGSVARLR^{70} was shown to impair the interaction of PimA with PI aggregates *in vitro*.[6]

Figure 2C showed that the mannose moiety of PIM is stabilized by the H-bond and electrostatic interactions of residues E199, G273, and E274, whereas the inositol moiety of PIM interacted with the residues Y9 and N97. The residues E199, G273, and E274 were involved in binding the mannose moiety of PIM (Figure S3), similar to binding the mannose part of GDPM in the crystal structure of PimA, which further strengthens that the docked structure can be a very good prediction. In addition, deletion of the residue Y9 was shown to be detrimental to the mannosyltransferase activity of PimA.[6] The residue N97 formed a hydrogen bond with the O4 atom of inositol. The residue R201 of PimA formed an ionic interaction with the phosphate group of PIM, suggesting a possible critical role of this residue in binding PIM. The residues P8, S10, L56, F71, and P99 interacted with one acyl chain of PIM, whereas the residues E95, A98, F130, and Q131 stabilized the other acyl chain of PIM. Based on these docking analyses, we can hypothesize that the residue R201 is very critical for binding both PI and PIM and the mannose transfer mechanism of PimA. The residues 59−70, contain a few residues that can stabilize an acyl chain of PI. A few segments of the N-terminal part of PimA, such as residues ^{8}PYS^{10} and P40, residue ^{95}EXAP^{99}, and residues 121−131 interacted with the acyl chains of PI and PIM. To check the stability of the docked complexes, we performed molecular dynamics simulations of the docked structures of PI and PIM with PimA in the following section.

3.3. Molecular Dynamics Simulations. *3.3.1. Root-Mean-Square Deviation (RMSD) Analyses.* To investigate the stability of the docked structures of PI- and PIM-bound PimA, molecular dynamics (MD) simulation studies were conducted for a time duration of 300 ns. Solvent pH was considered to be 7.5 to mimic the experimental conditions of earlier studies on PimA.[6,18,40] The available crystal structures of GDP- and GDPM-bound PimA were also subjected to MD simulations at pH 7.5. In addition, coordinates of PI and GDPM were obtained from the docked structure and crystal structure, respectively, and they were superposed hoping the MD simulation with both the substrates may reveal how PimA facilitates the mannose transfer reaction at the catalytic site. Similarly, coordinates of PIM and GDP were also obtained and superposed together with PimA to investigate how PimA interacts with both the products near the catalytic site.

Root-mean-square deviations (RMSDs) of the protein backbone atoms were calculated to examine the stability of the global structure of PimA in the free form and in ligand-bound forms (Figure 3A). Measurement of the radius of gyration (R_g) provides an estimate of the compactness of a protein structure. The changes in the R_g values of PimA and various ligand-bound PimA are plotted in Figure 3B. Average RMSD and R_g values of all of the PimA structures are shown in Table 1A.

3.3.1.1. PimA Adopts Two Different Conformations. It can be observed from Figure 3A that the RMSD values of the PimA structure remained relatively high from 140 to 230 ns, indicating that the backbone stability was relatively less during this time. Investigation of the representative structures revealed that PimA adopts a relatively open conformation at this period.

https://doi.org/10.1021/acsomega.2c00832
ACS Omega 2022, 7, 19288−19304

Table 1. Values Derived from the RMSD, PCA, and RMSF Measurements of PimA and Ligand-Bound PimA as Obtained from Molecular Dynamics Simulations[a]

		PimA	PimA-GDPM	PimA-GDP	PimA-PI	PimA-PIM	PimA-PI-GDPM	PimA-PIM-GDP
A.	backbone RMSD (Å)	6.33 ± 2.62	3.87 ± 1.28	3.12 ± 0.49	3.87 ± 0.97	4.78 ± 0.90	2.61 ± 0.31	3.71 ± 0.71
	R_g (Å)	24.52 ± 1.20	23.33 ± 0.66	22.95 ± 0.31	23.38 ± 0.59	23.05 ± 0.34	22.65 ± 0.18	23.03 ± 0.39
B.	contribution to variance by eigenvector 1	69.56%	52.44%	26.01%	50.53%	41.67%	20.66%	30.38%
	contribution to variance by eigenvector 2	7.76%	11.98%	15.44%	12.52%	13.32%	15.88%	19.98%
	sum of the eigenvalues of all eigenvectors	48.25	20.46	12.26	18.16	17.70	7.07	9.49
C.	significantly decreased compared to PimA		^{42}SP^{43}, K46, **L69**, A158, L159, A173, D232	**L69**, D232, E236	A173, ^{231}ED^{232}, E236, ^{239}GD^{240}	**L69**, D232, E236	^{12}DV^{13}, ^{41}ASPHV^{45}, V58, **L69**, Q155, A158, D232, E236, G239	^{155}QMEAL^{159}, R228, D232
	significantly increased compared to PimA		**R201**, ^{293}SD^{294}, ^{310}LVP^{312}	F130, L134, W154, ^{156}ME^{157}, L159	W154, **R201**, K202, H270	^{125}**LTLSVF**^{130}, ^{153}RW^{154}	R358	Q131

[a]A. The average RMSD values of the backbone atoms and the average R_g values of PimA along with its different ligands GDPM, GDP, PI, PIM, GDPM +PI, and GDP + PIM. B. Contribution of the eigenvalues of top two eigenvectors and sum of all of the eigenvalues derived from PCA. C. Significant changes in the RMSF values due to the presence of various ligands with PimA. Residues marked in bold play significant roles in binding the ligands. Mobility of the residue L69 was significantly more constrained due to the presence of GDPM/GDP/PIM/PI+GDPM. The residue R201 shows higher mobility due to the presence of GDPM/PI. The residues ^{125}LTLSVF^{130} show higher mobility in the presence of PIM.

This observation corroborates the notion that PimA can assume two conformations, *i.e.*, open and closed, by supporting previous experimental findings from SAXS, disulfide linkage, and crystallographic analyses.[18,42] Average RMSD and R_g values of PimA were found to be 6.33 ± 2.62 and 24.52 ± 1.20 Å, respectively. To get a better estimation of the R_g values of PimA in two different conformations, average R_g values were calculated for 150−230 ns and for 1−140 and 240−300 ns, as the representatives of the open and closed conformations, respectively. Average R_g values of the open and closed conformations of PimA were found to be 26.29 ± 0.28 and 23.79 ± 0.54 Å, respectively, indicating a significant change in the conformations. In another study, using SAXS data, R_g values were estimated to be 28.5 and 27.5 Å for PimA and GDP-bound PimA, respectively.[42] In our work, the average R_g value of GDP-bound PimA was found to be 23.33 ± 0.66 Å, more compact than the closed conformation of PimA, agreeing with the observation that binding of GDP promotes more compact conformation of PimA.[42] The "Rossmann fold" domains of PimA form a cleft where most critical residues for catalysis are present.[16] Interdomain movements during glycosyl transfer reactions were shown or predicted in other enzymes containing GT-B folds, such as MurG,[43] glycogen synthase,[44,45] and MshA.[46] The differences in two conformations of PimA are shown by comparing two representative snapshots from the MD simulation in Figure 4. In Figure 4A,B, snapshots of PimA at 100 and 200 ns have been shown that represent closed and open conformations, respectively. It can be observed that the distance between two catalytically important residues, R68 and R201, is 34.5 Å in the closed conformation, whereas this distance is 51.1 Å in the open conformation. Residues G64 and E231 are located at the end of the catalytic pocket and can be considered two endpoints of the pocket for this analysis. Their distance changed from 29.7 to 51.2 Å when PimA shuffled its structure from the closed to open conformation. The residues D329, W349, and A366 form an angle of 141.0° in the closed conformation; however, this angle decreases to 115.6° in the open conformation. This angle may be considered a representative of the hinge that opens and closes the PimA conformation. We further investigated the variation of this angle during the simulation (Figure S4). Similar to the RMSD and R_g analyses, a period of dip in the values of the angle can be observed during 140−230 ns, indicating an open conformation of PimA (Figure S4-A). Further inspection of the values of this angle revealed two distinct populations of the angles where the open and closed conformations of PimA showed peaks at 115 and 145°, respectively (Figure S4-B). This result is apparently contrasting to a recent experimental work,[20] which showed that the nucleotide part and β-PO_4^{2-} of GDPM is responsible for facilitating "open to closed motion" of PimA, whereas our results show that PimA itself can fold back to the closed conformation. It may be possible that the "closed to open" motion of PimA is partially inhibited in the presence of GDPM due to its nucleotide moiety and β-PO_4^{2} group.

3.3.1.2. GDP-Bound PimA Is Most Compact When Only One Ligand Is Bound. It can also be observed from Figure 3A and Table 1A that the RMSD values of the backbone residues of PimA are relatively higher than the RMSD values of ligand-bound PimA structures. The average RMSD values of GDPM- and GDP-bound PimA were, respectively, 3.87 ± 1.28 and 3.12 ± 0.49 Å. This indicates that the backbone structure of PimA stabilizes with the presence of GDPM and GDP, which is

https://doi.org/10.1021/acsomega.2c00832
ACS Omega 2022, 7, 19288−19304

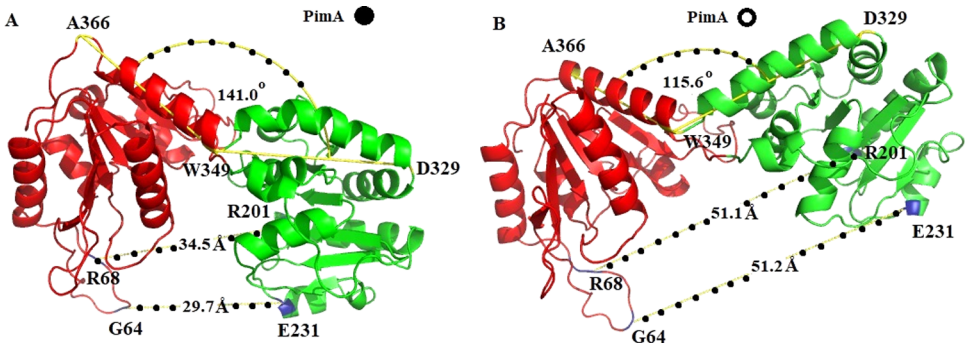

Figure 4. "Closed" and "open" conformations of PimA as were obtained from the snapshots from MD simulations. A. At 100 ns (closed conformation) B. At 200 ns (open conformation). (A) and (B) show the overall structural differences between the "closed" (marked with a filled circle) and "open" conformations (marked with an empty circle). The distance between the C_α atoms of R68 and R201, G64 and E231, and the angle formed among D329, W349, and A366 vary in two different conformations. The N-terminal and C-terminal domains are colored in red and green, respectively. Residues for distance measurement and the residues for angle measurement are shown in blue and yellow, respectively.

consistent with the previous observations on PimA.[42] The average R_g values of GDPM- and GDP-bound PimA were, respectively, 23.33 ± 0.66 and 22.95 ± 0.31 Å, comparatively much lower than the average R_g value of the open conformations, *i.e.*, 26.29 ± 0.28 Å, and slightly lower than the average R_g value of the closed conformations, *i.e.*, 23.79 ± 0.54 Å. The RMSD and R_g values indicate that the GDP-bound structure is slightly more stabilized than the GDPM-bound PimA, which is consistent with the previous experimental observations from the isothermal titration calorimetry (ITC) measurements,[6] which showed that the K_d values of GDP binding (0.31 μM) were lower compared to binding of GDPM (2.27 μM), indicating that the binding of GDP further stabilizes PimA than the binding of GDPM. Although the active sites of both the ligands coincide, the presence of extra polar groups on the mannose moiety near E274 and S275 may cause slight destabilization of PimA compared to GDP. This little lower stability of PimA with GDPM may help in the overall scheme of mannose transfer from GDPM to PI to form a stable product GDP and another product PIM, which binds to the N-terminal more favorably than PI (Section 3.2). The lower standard deviations of the RMSD and R_g values indicate relatively less structural deviation of GDP-bound than free and GDPM-bound PimA. Our study also supports a previous SAXS study,[42] which showed that GDP induces closing movement of PimA. From Table 1A and Figure 3A,B, we can also infer that both PI- and PIM-bound PimA structures are more stabilized than the PimA structure. The average RMSD value of the PimA backbone atoms while bound to PI was 3.87 ± 0.97 Å, similar to that of GDPM-bound PimA. The relatively higher average RMSD values (4.78 ± 0.90 Å) of PIM-bound PimA indicated that PIM-bound PimA has relatively more backbone movement, which may help PimA to deliver the product from the catalytic site to the cytoplasm/inner membrane. Overall, when only one ligand is bound, RMSD and R_g analyses indicate that the binding of GDP promotes the most compact structure of PimA, whereas binding of PIM destabilizes the PimA backbone the most.

3.3.1.3. PimA Adopts the Most Compact Conformation When Both GDPM and PI Are Bound. It can also be observed from Table 1A that the binding of both PI and GDPM stabilizes the backbone dynamics of PimA further than when it was bound to PI alone, agreeing with the previous ITC measurements.[6] The average RMSD value of the backbone atoms and R_g value of PimA, while bound to both PI and GDPM, were 2.61 ± 0.31 and 22.65 ± 0.18 Å, respectively. This indicates that the presence of both the substrates makes PimA adopt the most compact conformation with much lesser deviation compared to interacting with any other ligand/ligands. This closed conformation of PimA may help bring the substrates PI and GDPM together to facilitate the mannose transfer reaction. Similarly, closed conformation had been shown to favor the catalytic steps of MshA of *Corynebacterium glutamicum*[46] and glycogen synthase of *Escherichia coli*.[45] Further QM/MM studies may help us elucidate if those close contacts may proceed to transfer the mannose group from GDPM to PI. The overall backbone flexibility (average RMSD value: 3.71 ± 0.71 Å) increased and the compactness decreased (average R_g value: 23.03 ± 0.39 Å) for PimA, when both the products GDP and PIM are bound, compared to when both the substrates GDPM and PI are bound, which probably helps to release the products from the active site of PimA.

3.3.2. Principal Component Analysis. The activity of an enzyme is often correlated with its dynamic properties.[47] Principal component analysis (PCA) of molecular dynamics trajectories can reveal essential dynamic properties. PCAs were carried out on PimA and ligand-bound PimA. Eigenvectors derived after diagonalizing the covariance matrix of C_α coordinates from PCA were sorted by their eigenvalues from highest to lowest, and cumulative contributions to variance of top 20 eigenvectors are plotted in Figure 5A. The contribution of the top two eigenvectors and the sum of all of the eigenvalues for PimA and all of the ligand-bound PimA are shown in Table 1B. Figure 5A shows that even though the total motion of the C_α atoms of PimA is dispersed over 1119 eigenvectors, 72−93% of the collective motions stemmed from the top 10 eigenvectors sorted by their corresponding eigenvalues. It can be observed from Table 1B that the top two eigenvectors contributed to 77.32% for PimA, whereas they contributed to 64.42, 41.45, 63.05, 55.00, 36.54, and 50.37% of the overall motions of PimA while bound to GDPM, GDP, PI, PIM, both GDPM and PI, and both GDP and PIM, respectively. The binding of ligands restricts the overall collective motions of PimA, and thus, a greater number of eigenvectors are required to represent the overall dynamics while bound to the ligands. This result also indicates that the binding of GDP has the largest damping effect on the most dominant motion represented by eigenvector 1 among all of the ligands when bound alone. This supports the RMSD and

https://doi.org/10.1021/acsomega.2c00832
ACS Omega 2022, 7, 19288−19304

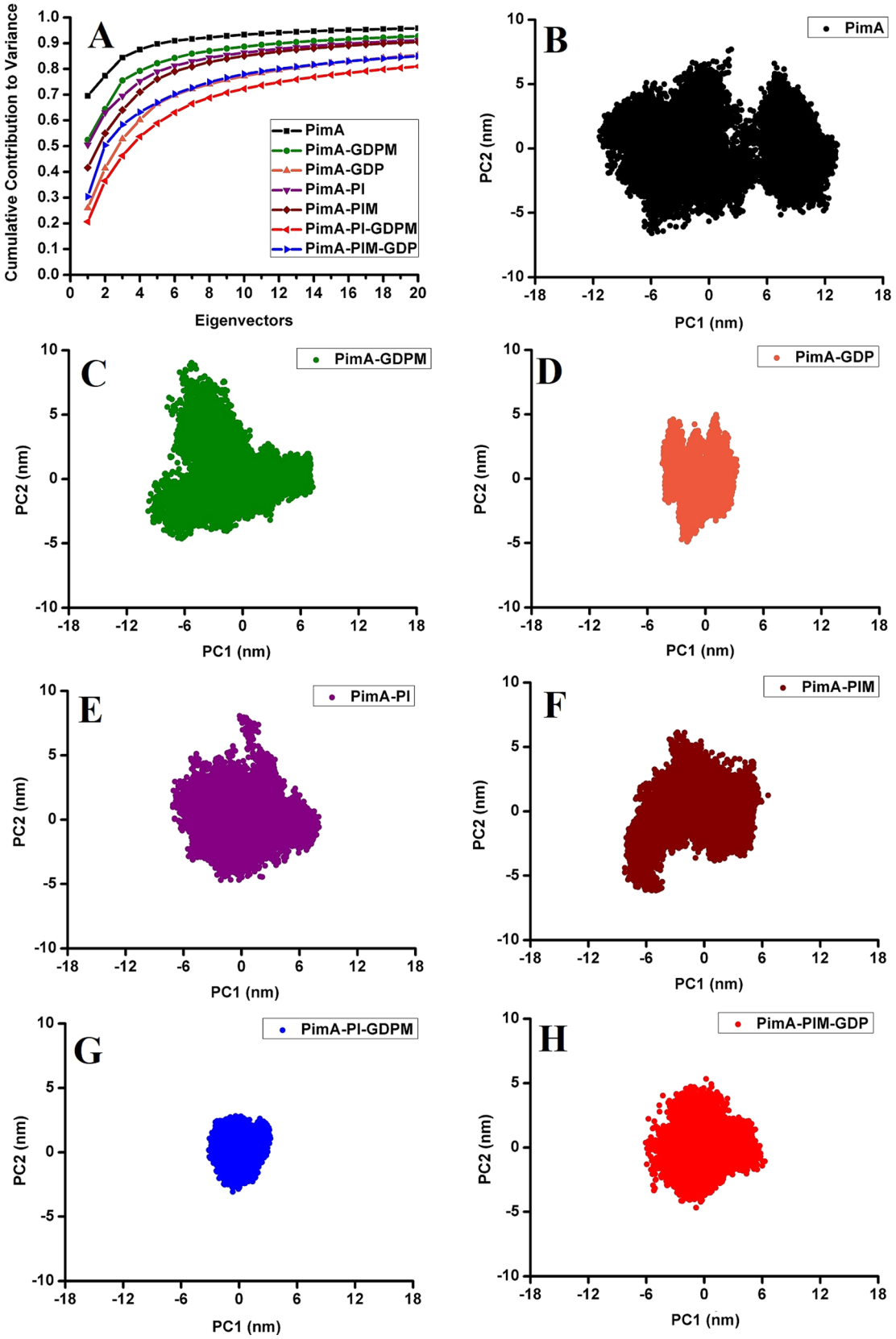

Figure 5. Principal component analyses (PCA) of PimA and ligand-bound PimA. (A) Cumulative contribution of the top 20 eigenvectors to the variance of overall motion of PimA. (B−H) Two-dimensional scatter plots of PC1 and PC2. (B) PimA. (C) GDPM-bound PimA, (D) GDP-bound PimA, (E) PI-bound PimA, (F) PIM-bound PimA, (G) GDPM + PI-bound PimA, and (H) GDP + PIM-bound PimA. PimA is the most flexible (B), but while bound to GDP (D), PimA assumes the least flexible conformation (when only one ligand is bound). When both GDPM and PI are present (G), PimA was least flexible; however, mobility of PimA increased relatively when both GDP and PIM are present (H).

https://doi.org/10.1021/acsomega.2c00832
ACS Omega 2022, 7, 19288−19304

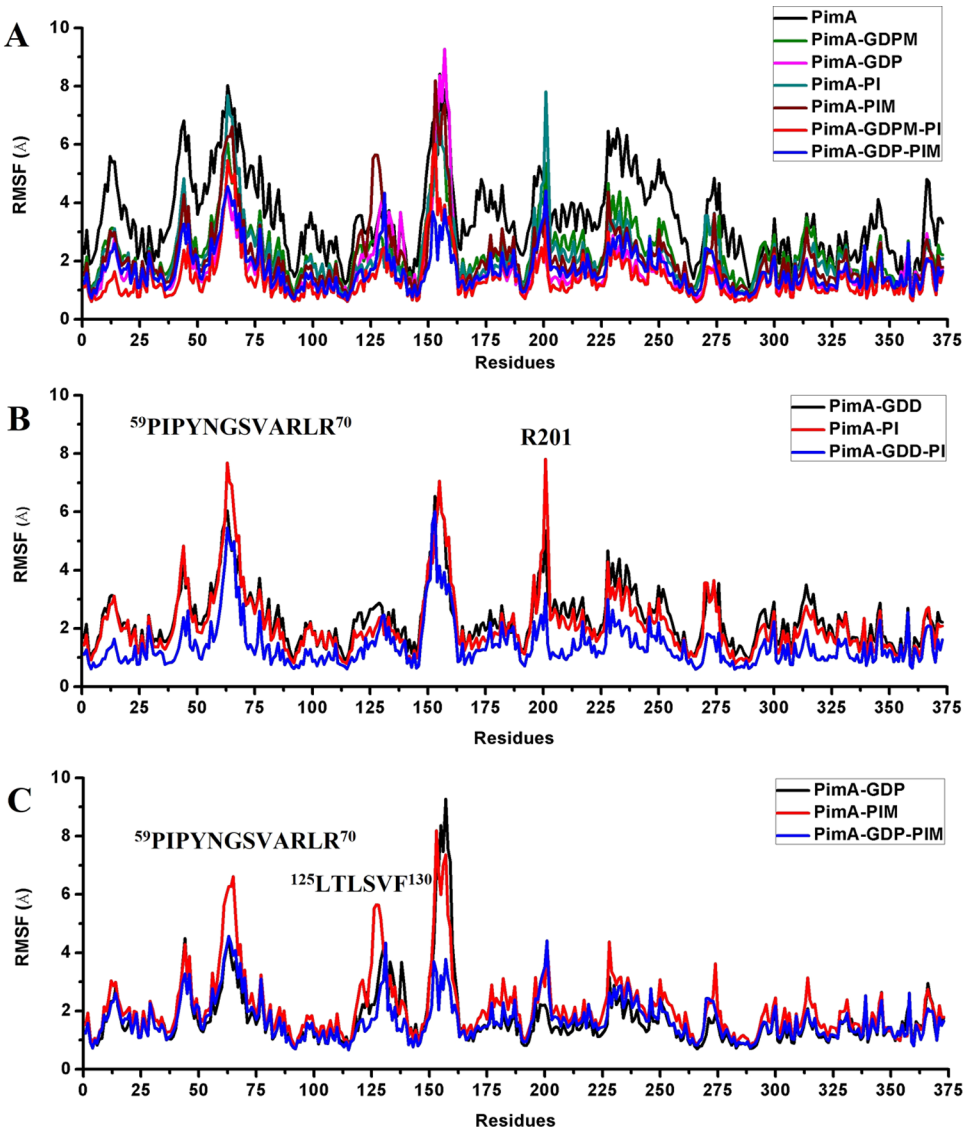

Figure 6. RMSF analyses of PimA and ligand-bound PimA. (A) RMSF values of PimA and PimA bound to GDPM, GDP, PI, PIM, GDPM + PI, and GDP + PIM. (B) RMSF values of PimA bound to the substrates, individually and together. (C) RMSF values of PimA bound to the products, individually and together. In general, residues of PimA are more flexible than that of any ligand-bound PimA (A). R201 has higher RMSF values when bound to GDPM or PI, but the value decreases when both GDPM and PI are bound. Binding of PI increases the RMSF values of the residues 59−70 of PimA (B). Binding of PIM increases the RMSF values of the residues 59−70 and 125−130 of PimA. The mobility of the residues 59−70, 120−131, and 149−162 decreases when both the products are bound (C).

R_g analyses (Section 3.3.1.2), which showed that GDP stabilizes and promotes the most compact conformations of PimA. The binding of both GDPM and PI has the lowest contribution to variance suggesting that while both substrates are bound, collective global motion is not as dominated by the top two eigenvectors as was in PimA, similar to the observations made by RMSD and R_g analyses in Section 3.3.1.3. The binding of both the products, *i.e.*, PIM and GDP, results in stronger collective motions, compared to while bound to both the substrates, *i.e.*, GDPM and PI.

The sum of the eigenvalues of all of the eigenvectors provides a quantitative analysis of the overall flexibility of a protein molecule. We find that this sum of the eigenvalues for PimA, and GDPM-, GDP-, PI-, PIM-, PI-GDPM-, and PIM-GDP-bound PimA are 48.25, 20.46, 12.26, 18.16, 17.10, 7.07, and 9.49, respectively. A comparatively larger sum of the eigenvalues indicated that PimA is very flexible in comparison to any ligand-bound PimA, matching with the observations made by RMSD and R_g analyses in Section 3.3.1.1. To visualize the essential subspace of collective motions of PimA with or without the ligands, principal components (PCs) 1 and 2 for PimA and various ligand-bound PimA are plotted in Figure 5B−H. It can be observed from Figure 5B−F that the binding of ligands reduces the flexibility of PimA along both eigenvectors 1 and 2. The binding of GDP showed the least flexibility with respect to the motions represented by these two eigenvectors compared to all of the other ligands bound alone. The binding of the substrate GDPM alone showed more flexibility than the binding of the product GDP, which may help facilitate the incorporation of the other substrate PI at the active site. It can also be observed from Figure 5G,H that the presence of both the substrates restricted the flexibility along both the eigenvectors most, whereas the binding of both the products promoted more flexibility to PimA. Combining with

https://doi.org/10.1021/acsomega.2c00832
ACS Omega 2022, 7, 19288−19304

the previous RMSD and R_g analyses, it can be said that when bound to both the substrates, PimA is more closed and least flexible, whereas it is more open and dynamic while bound to both the products. The closed conformation of PimA with the substrates may help in promoting the mannose transfer reaction in the active site, whereas the open conformation may help release the products from the active site.

3.3.3. Root-Mean-Square Fluctuation (RMSF) Analyses. Root-mean-square fluctuation (RMSF) values are used to calculate the average fluctuation in the position of an atom or a group of atoms during the course of an MD simulation, and thus are often considered as very good indicators of flexibility for protein residues. Comparisons in the RMSF values of various ligand-bound PimA with PimA are shown in Figure 6A. Differences in the RMSF values of ligand-bound PimA from PimA were also calculated, and deviations in RMSF values falling outside the range of mean ± 2 × s.d. (standard deviation) are reported in Table 1C.

3.3.3.1. Residues of PimA Are More Flexible. RMSF analyses showed that PimA has higher RMSF values for most of the residues than any ligand-bound PimA (Figure 6A), indicating that the overall mobility of PimA decreases in the presence of the ligands PI, PIM, GDP, GDPM, PI-GDPM, and PIM-GDP, which is consistent with our RMSD-R_g (Section 3.3.1.1) analyses and PCA (Section 3.3.2).

3.3.3.2. Loop Regions and Residues 147−162 Show High Mobility. The residues 9−16, 41−49, 56−71, 118−123, 177−188, 217−220, 248−252, 270−277, 311−317, and 365−370 of PimA are known to form disordered regions from previous crystallographic studies,[6,18] which explains relatively higher RMSF values of these residues in general (Figure 6A). In each simulation, there is a large peak corresponding to the residues 147−162, which may be attributed to the fact that this study was based on the crystal structure obtained from the PDB entry4N9W, where residues 149−162 were missing.[18] However, in another crystal structure of PimA (PDB entry:2GEK), the residues 148−161 formed a (α6) helical structure.[6] All residues of this region showed relatively higher RMSF values possibly due to their modeled random coil structure. Some of the residues which lie between 149−162 showed higher mobility while binding to GDP and PIM than PimA (Figure 6C). Many residues which belong to the region 149−162 of PimA exhibited higher mobility than PimA while interacting with GDP, PI, and PIM, but only W154 showed higher mobility when bound to GDPM (Table 1C). This shows that this region interacts differently when bound to GDPM than when bound to PI, PIM, or GDP.

3.3.3.3. Residue R201 of PimA Is Flexible in the Presence of GDPM and PI. Previous mutational studies demonstrated important roles of the residues Y9, Q18, Y62, N63, R68, ^{77}RKVKK^{81}, H118, R196, E199, R201, and E274 in the mannosyltransferase activity of PimA.[40] The residue R201 of PimA showed higher RMSF values than PimA in the presence of either GDPM or PI, indicating greater flexibility during the MD simulation (Figure 6B). Our multiple sequence alignment (Section 3.1) and docking analysis (Section 3.2) predicted a critical role for the residue R201 of PimA with PI and PIM. Previous docking analysis also predicted a critical role of R201 in binding PI.[6] Interestingly, with GDP, the residue R201 of PimA was not as mobile during the course of the MD simulation as it was in the case with GDPM. Possibly, the presence of GDPM or PI induces a change in PimA where R201 becomes more mobile, which may help the guadinium group of R201 to interact with either the phosphate group of PI or to form H-bonds with the hydroxyl groups of the inositol group of PI, which may further facilitate the mannose transfer reaction.

3.3.3.4. Residues 59−70 Except L69 of PimA Is Mobile While Bound to PI or PIM. The residues 59−70 of PimA, consisting of the β3-α2 loop, showed comparatively higher values when bound to PI or PIM than when bound to GDP or GDPM (Figure 6B,C). This indicates that these residues become more mobile while interacting with PI or PIM. The ligands PI or PIM may move along with these residues during simulation. The residue L69 showed significantly low RMSF values while bound to GDP, GDPM, PIM, and PI-GDPM than PimA alone, indicating confinement of this residue (Table 1C). GDPM and GDP both bind predominantly to the C-terminal residues. However, binding of GDPM and GDP both lowered the dynamic motion of the residue L69, as revealed by the RMSF values (Table 1C), indicating allosteric communication. This residue L69 is also important for binding both PI and PIM as will be shown later (Section 3.3.4.2). Docking analyses indicated that L69 interacts with the acyl chain of PI (Section 3.2). Lower mobility of this residue in the presence of GDPM and GDP suggests that this residue may be crucial to capture the hydrophobic acyl chain of PI or PIM. Lowered dynamic motion of L69 may help PimA to bind to PI or PIM by the loop residues 59−70. Previously it was shown that the loop consisting of the residues 59−70 of PimA is crucial to interact with PI aggregates.[6] RMSF analyses showed that this loop becomes mobile while interacting with PI or PIM, except the residue L69, which is confined when PimA is bound to any substrate or product.

3.3.3.5. Higher Mobility and Allosteric Communication. The residues F130 and R134 demonstrated higher mobility while interacting with GDP than free PimA (Table 1C). Similarly, residues 125−130 of PimA showed higher mobility in the presence of PIM than PimA (Table 1C and Figure 6C). Previously it had been shown that residues 129−163 exhibit notable conformational changes.[18] The residue Q131 of PimA showed higher mobility than PimA in the presence of both the products. The residues 125−131 may have a significant role in releasing the product PIM from the active site. Apart from R201, the residue K202 of PimA, known to bind the β-phosphate of GDPM,[6] also showed higher mobility in presence of PI, which further strengthens its role in the mannose transfer reaction.

RMSF analyses indicated (Table 1C) that the binding of GDPM significantly lowers the dynamic motion of the residues S42, P43, K46, A158, and L159, whereas binding of GDP significantly increases the dynamic motions of the residues F130, L134, W154, M156, E157, and L159. This indicates that binding of GDP and GDPM shows a change in the dynamic motions of various N-terminal residues of PimA. The binding of PI and PIM also changed the dynamic motions of a few residues of the C-terminal domain, as is observed by the RMSF values. Thus, our MD analyses indicate allosteric communication between the two domains induced by ligand binding.

3.3.4. Molecular Mechanics Generalized Born Surface Area Analyses. 3.3.4.1. Binding of GDP with PimA Is Most Stable. The free energy of binding, *i.e.*, ΔG_{bind}, for each of the substrates, *i.e.*, PI and GDPM, and the products, *i.e.*, PIM and GDP, of PimA were calculated by Molecular Mechanics Generalized Born Surface Area (MMGBSA) analyses using the gmx_MMPBSA software.[39] Snapshots for MMGBSA analyses

https://doi.org/10.1021/acsomega.2c00832
ACS Omega 2022, 7, 19288−19304

were taken at an interval of 1 ns of the 300 ns long MD simulations. The values of ΔG_{bind} and previous estimations of K_d and ΔG_{bind} are shown in Table 2. The ΔG_{bind} values for GDP-bound (−36.10 ± 10.17 kcal/mol) are the lowest in comparison to GDPM-bound (−26.63 ± 9.94 kcal/mol) and PI-bound (−21.81 ± 9.47 kcal/mol) PimA, which agrees with the previous estimation of dissociation constant K_d from the isothermal titration calorimetry measurements.[6] This observation indicates that the binding of GDP with PimA led to the formation of the most stable complex, compared to the binding of GDPM and PI, which is also shown in our previous RMSD, R_g, and PCA (Sections 3.3.1.3 and 3.3.2). MMGBSA analyses also showed that the ΔG_{bind} between PimA and PIM is −19.45 ± 6.29 kcal/mol, which is in a similar range to PimA and PI.

Table 2. Comparison of the ΔG_{bind} Values Obtained from MMGBSA Analyses (This Work) and ITC Measurements[6] of Various Ligands with PimA[a]

	ΔG_{bind} from MMGBSA analyses (kcal/mol)	K_d and ΔG_{bind} values from ITC measurements[6]	
		K_d (μM)	$\Delta G_{bind} = -RT \ln(K_d)$ (kcal/mol)
GDPM	−26.63 ± 9.94	0.23	−0.87
GDP	−36.10 ± 10.17	0.03	−2.08
PI	−21.81 ± 9.47	2.27	−0.48
PIM	−19.45 ± 6.29	NA	NA

[a]NA: Not Available.

Thus, there is not much difference in the binding energies between PI and PIM with PimA as estimated from the MMGBSA analyses, whereas the binding of GDP is slightly favored over the binding of GDPM. Overall, this lower ΔG_{bind} between PimA and GDP may drive the mannose transfer reaction forward. Based on the ΔG_{bind} derived from the MMGBSA analyses, it can probably be safe to hypothesize that PIM will be released first and then GDP when both PIM and GDP are bound to PimA. Similarly, the ΔG_{bind} of GDPM is lower than that of PI with PimA, which indicates that possibly GDPM is recruited to PimA first and then PI is recruited.

3.3.4.2. Residue Decomposition Analyses. Residue decomposition of MMGBSA analyses of various ligand-bound PimA structures were attempted to figure out which residues contributed the most to ligand binding (Figure 7). Previously, it was shown that the residues P14, L194, G227, D253, and K256 stabilize the guanine ring; the residues G15, D252, D253, K256, and E282 interact with the ribose sugar; the residues G16, R196, and K202 interact with the β-phosphate of GDPM; and the residues E274, S275, F276, and I278 interact with the mannose group of GDPM. Figure 7A shows that residues R196, K202, and R228 of PimA contributed the most to binding GDPM. The residue R228 of PimA stabilizes the guanine base of GDPM by π-cation interactions. The residues ^{13}VPGG^{16}, ^{194}LG^{195}, G227, ^{250}QV^{251}, ^{274}ESF^{276}, and ^{278}IV^{279} also showed favorable ΔG in binding GDPM, demonstrating that the residues closer to the known interaction sites play crucial roles. It should also be noted that the residues E95, E199, and E282 showed slightly unfavorable ΔG_{bind}, which

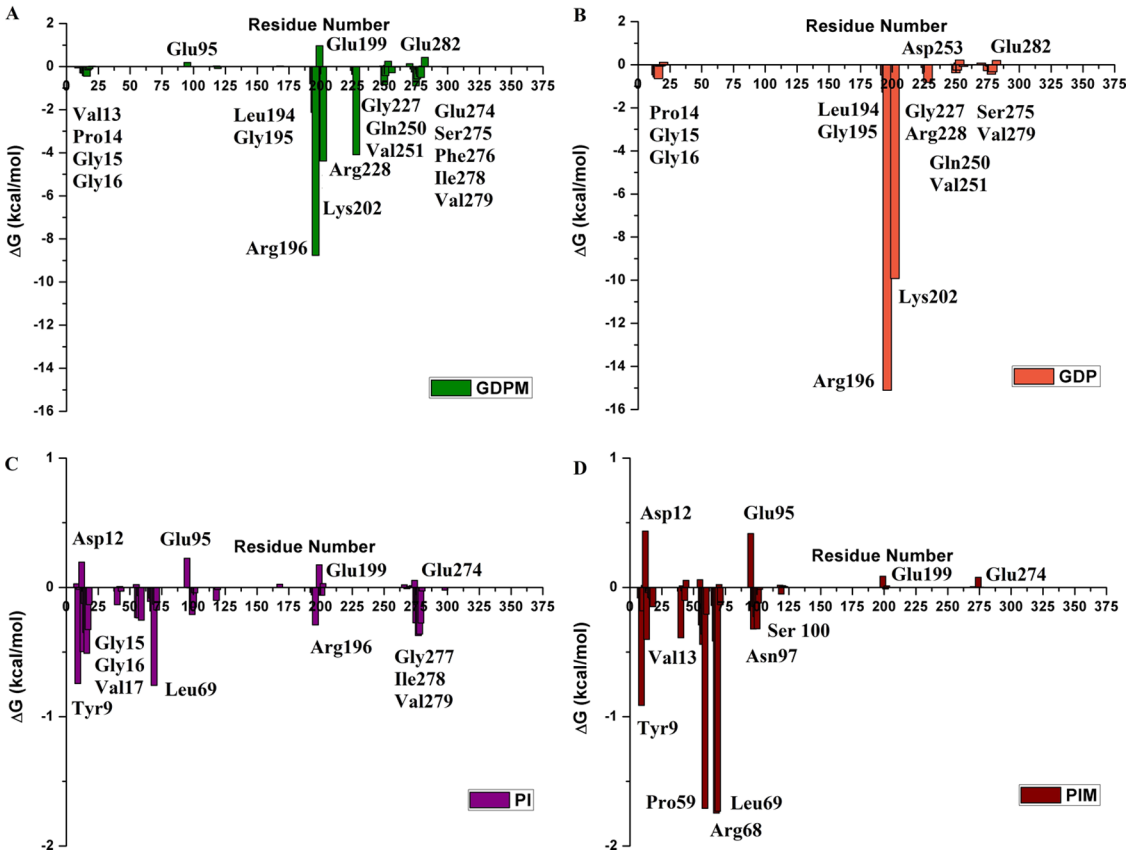

Figure 7. Residue-specific MMGBSA analyses of various ligand-bound PimA. (A) GDPM-bound, (B) GDP-bound, (C) PI-bound, and (D) PIM-bound. R196, K202, and R228 strongly interacted with GDPM (A). R196 and K202 interact strongly with GDP (B). Y9, ^{15}GGV^{17}, L69, and ^{277}GIV^{279} showed strong interactions with PI (C). Y9, V13, P59, R68, L69, and N97 showed strong interactions with PIM (D).

https://doi.org/10.1021/acsomega.2c00832
ACS Omega 2022, 7, 19288−19304

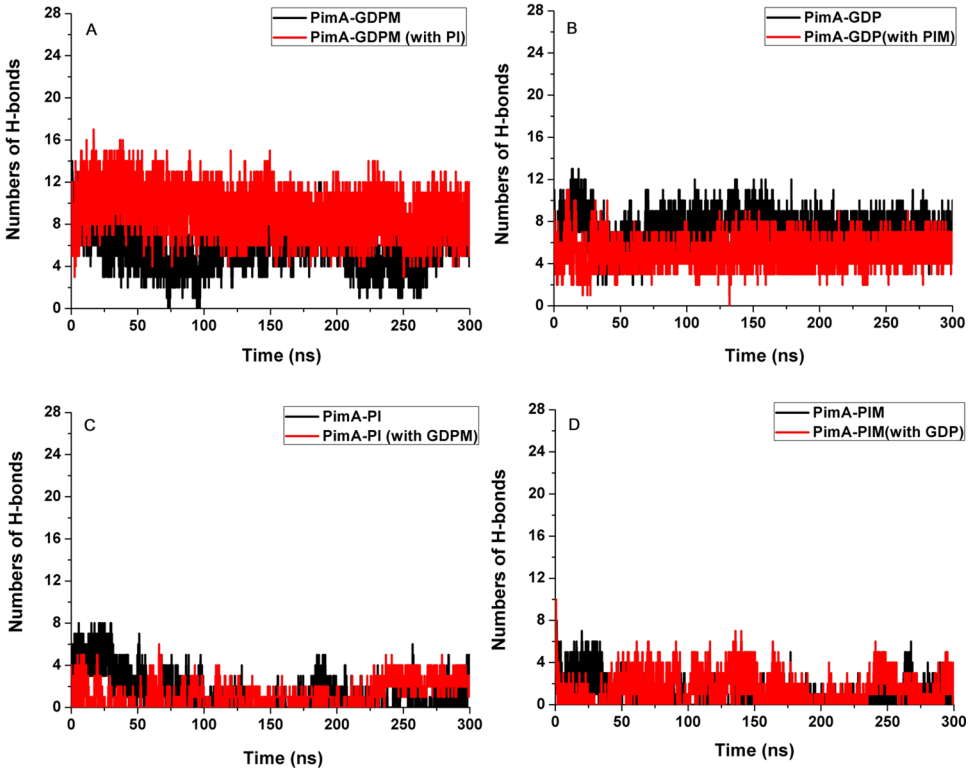

Figure 8. Average number of H-bonds during the MD simulations between PimA and various ligands. (A) With GDPM in the presence and absence of PI. (B) With GDP in the presence and absence of PIM. (C) With PI in the presence and absence of GDPM. (D) With PIM in the presence and absence of GDP. The presence of PI increased the number of H-bonds between PimA and GDPM (A), whereas the presence of PIM decreased the number of H-bonds between PimA and GDP (B). The presence or the absence of GDP/GDPM does not significantly affect the number of H-bonds between PI/PIM with PimA (C, D).

probably arises from the unfavorable packing of the negatively charged side chains in a hydrophobic environment. Similarly, Figure 7B shows that D253 and E282 exhibited slightly unfavorable ΔG_{bind}, whereas residue ^{14}PGG^{16} and residues ^{194}LGR^{196}, K202, ^{227}GR^{228}, ^{250}QV^{251}, S275, and V279 showed favorable ΔG_{bind} while binding to GDP. It should be noted that R196 and K202 of PimA showed much tighter binding to GDP than to GDPM, and this may contribute to the overall favorable binding of GDP over GDPM. The strong binding between the residues R196 and K202 of PimA with GDP explains why PimA adopts the most stabilized and most compact conformation of PimA, as was shown in RMSD-R_g analyses and PCA.

We also investigated the role of the residues in binding PI and PIM, and it was found that residues D12, E95, E199, and E274 of PimA show slightly unfavorable ΔG_{bind} while binding to both PI and PIM (Figure 7C,D). Previous docking and mutation studies predicted an important role of Y9 residue in binding the substrate PI[6]. Here, both PI and PIM interact favorably with Y9 and its role in binding PI and PIM is strongly supported. The residues V13, ^{15}GGV^{17}, ^{99}PS^{100}, H118, R196, and ^{277}GIV^{279} showed favorable ΔG_{bind}, suggesting their role in binding PI to PimA. The residue R196 may play a critical role in bringing both PI (Figure 7C) and GDPM (Figure 7A) together as can be observed from these MMGBSA analyses. The residues 59−70 of PimA showed negative ΔG_{bind} values, indicating their role in binding PI (Figure 7C). A previous experimental study demonstrated that these residues are necessary for the mannosyltransferase activity and the ability of PimA to bind PI aggregates.[6] Among these residues, L69 showed the strongest binding to PI, supporting the previous observation from the RMSF analyses (Section 3.3.3.4). The residues 59−70 of PimA showed negative ΔG_{bind} with PIM, thus suggesting their role in binding PIM as well. Among these residues, the residues P59, R68, and L69 showed the most negative values of ΔG_{bind}, supporting their strong involvement in binding PIM. Thus, MMGBSA analyses indicated that the residues 59−70 of PimA play critical roles in binding both the substrate PI and the product PIM. The residues 97−102 also showed negative ΔG_{bind}, whereas the residues N97 and S100 showed stronger interactions with PIM, indicating that these residues also interact with PIM favorably. Docking analyses predicted that N97 stabilizes the inositol moiety of PIM, which explains favorable ΔG_{bind} with PIM.

In sum, residue decomposition of the MMGBSA analyses showed that the residues R196, K202, and R228 are very crucial while binding GDPM, whereas the residues R196 and K202 interact strongly to bind GDP at the active site of PimA. The residues Y9 and L69 also interacted with both PI and PIM. The residues P59, R68, and N97 also contributed strongly to binding PIM.

3.3.5. Hydrogen-Bond Analysis. Hydrogen bonds often determine the strength of interaction between a protein and a ligand. The docking analyses (Section 3.2) showed that the most stable conformation of PI and PIM formed one and two H-bonds, respectively. Hydrogen-bond analyses of protein−ligand complexes were carried out (Figure 8) on the MD trajectories to check if binding of one ligand promotes stronger binding of the other ligand or not. The average numbers of H-bonds of each ligand-bound complex of PimA are also shown

https://doi.org/10.1021/acsomega.2c00832
ACS Omega 2022, 7, 19288−19304

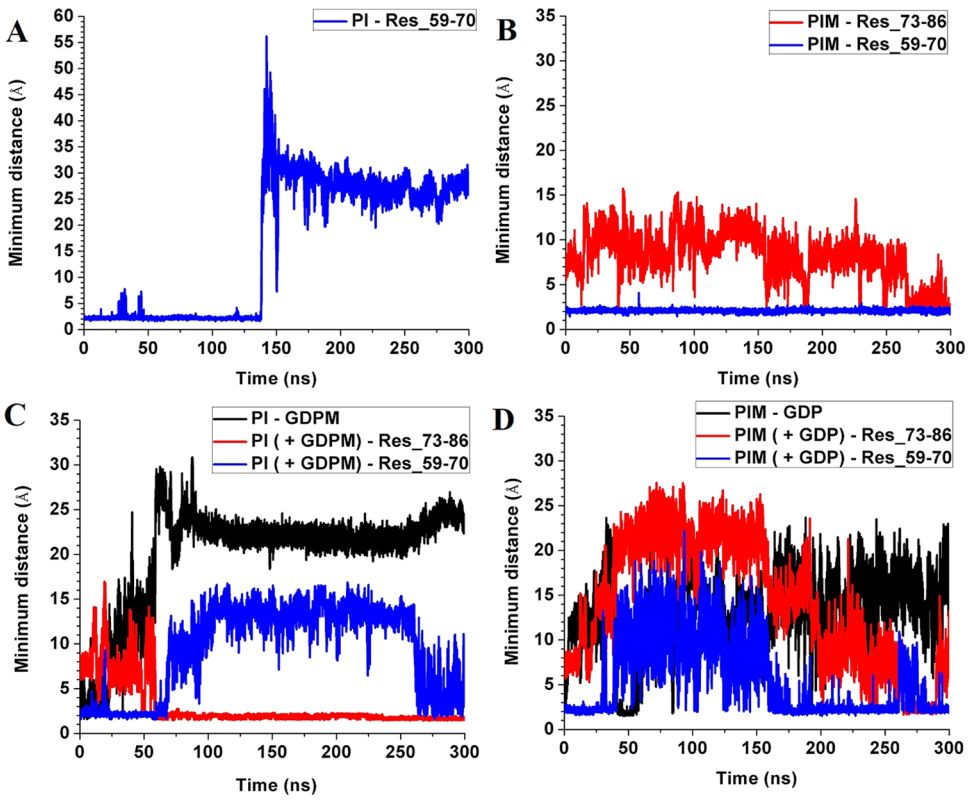

Figure 9. Minimum distance analyses of PI and PIM with various segments of PimA. (A). Between PI and residues 59−70. (B). Between PIM and residues 59−70/73−86. (C). Between PI and GDPM/residues 59−70/residues 73−86. (D). Between PIM and GDP/residues 59−70/residues 73−86. PI remained in close contact with the residues 59−70 of PimA for more than 135 ns, and then it detached from the active site of PimA (A). PIM remained in close contact with the residues 59−70 throughout, whereas it interacted with the residues 73−86 many times during the MD simulation. (C). PI and GDPM stayed in close contact for a brief period of time. PI interacted with the residues 59−70 up to ∼60 ns and remained in close contact with the residues 73−86 of PimA after 64 ns. (D). PIM interacted closely with GDP for a brief period of time (∼47−53 ns). PIM made contacts with the residues 59−70 often, whereas it interacted with the residues 73−86 of PimA between 270 and 290 ns.

in Table S2. The average number of H-bonds formed between GDPM and PimA is ∼6, but if PI is also present along with GDPM, the average number of H-bonds formed between PimA and GDPM is ∼9. As previously observed in RMSD and R_g analyses (Section 3.3.1.3), the presence of both the substrates led to the formation of the most compact and stable conformation of PimA. Although GDPM may form 12 H-bonds in the crystal structure,[6] it is very likely that many H-bonds are broken in the dynamic conformation. Even the PCA also showed that PimA is relatively more flexible in the presence of GDPM than in the presence of GDPM and PI both (Section 3.3.2). Inspection of the MD trajectories involving PimA and both GDPM and PI revealed that although the position of PI changes significantly than the docked position, the position of GDPM remains relatively stable during the course of the simulation. It can possibly be safe to say if GDPM is present at the catalytic site of PimA, the incorporation of PI strengthens the binding of GDPM further. However, the average number of H-bonds formed between PI and PimA remained unchanged (Figure 8C) irrespective of whether GDPM was present or not. Similarly, the average number of hydrogen bonds formed between the product PIM and PimA (Figure 8D) slightly increased with the addition of GDP in the active site, but it falls within one standard deviation. Furthermore, the presence of PIM was shown to decrease the number of H-bonds formed between GDP and PimA (Figure 8B). It can be observed from the PCA (Figure 5D,H) that the dominant motion along PC1 is relatively higher for PimA when it is bound to both GDP and PIM than GDP alone. However, the number of H-bonds formed during the MD simulation course remained in a similar range for both GDPM and GDP (Table S2). This raises a question about how the product GDP is released from the active site and how the substrate GDPM for the next catalytic cycle is reintroduced to PimA catalytic site. Overall, analyzing the number of H-bonds revealed that PI stabilized the binding of GDPM, whereas PIM slightly destabilized the binding of GDP with PimA.

3.3.6. Secondary Structure Transition. It had been shown that the residues 129−163 show significant structural changes, whereas helix α4, which consisted of residues 134−145, and helix α5, which consisted of residues 149−157, may transform into an extended conformation.[18] In this work, we observed that residues 120−140 show significant structural changes in GDP- and GDP-PIM-bound conformations of PimA (Figure S5A,B). A previous experimental study[18] also showed that at least one of the two tryptophan residues, W82 and W349, undergo significant structural change while interacting with membranes. We also noticed that the residue W349 remained disordered, whereas W82 remained a part of the α2 helix during the simulation (data not shown). This mobile W349 is part of the hinge region (Section 3.3.1.1) that helps move the two "Rossmann fold" domains in open and closed conformations, thus explaining why it is disordered. We also observed that the residues 59−70 (β3-α2 loop) of PimA undergo significant structural changes while interacting with PI (Figure S5C,D). Our analyses showed that these residues form

https://doi.org/10.1021/acsomega.2c00832
ACS Omega 2022, 7, 19288−19304

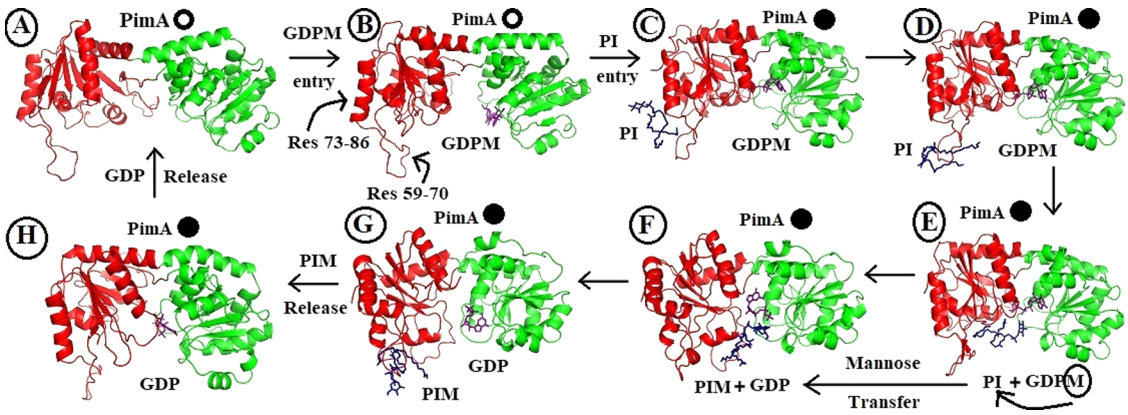

Figure 10. Hypothetical scheme of mannose transfer by PimA. A. Free PimA. B. GDPM-bound PimA. C. PI from the inner membrane interacts with the amphipathic α-helix residues 73−86 of GDPM-bound PimA. D. Residues 59−70 then help PI move to the catalytic site. E. Mannose transfer reaction is taken place at the catalytic site between GDPM and PI. F. PIM and GDP are formed at the catalytic site. G. Residues 59−70 may help PIM to transfer either to the residues 73−86 (amphipathic α-helix) or to the cytoplasm where PIM would be further mannosylated and acylated. H. GDP leaves the catalytic site at the end. Open and filled circles denote the open and closed conformations of PimA, respectively. Snapshots A, B, C−E, F−G, and H were obtained from the simulations of PimA (200 ns), PimA-GDPM (155 ns), PimA-PI-GDPM (64, 58.78, and 5.71 ns), PimA-PIM-GDP (51.95 and 249.54 ns), and PimA-GDP (300 ns), respectively.

a β-sheet structure while interacting with PI, indicating a stable interaction, which supports the docking (Section 3.2), RMSF (Section 3.3.3.4), and MMGBSA analyses (Section 3.3.4.2).

3.3.7. Analyses of Molecular Dynamics (MD) Trajectories. *3.3.7.1. PimA-PI.* Minimum distance analyses of the MD trajectories further supported the critical role played by residues 59−70 of PimA in binding PI. Figures 9A and S6 showed that PI interacts for the first ∼135 ns with the residues 59−70 during the MD simulation. This is further supported by previous molecular docking (Section 3.2), RMSF (Section 3.3.3), MMGBSA analyses (Section 3.3.4), and secondary structure transition analyses (Section 3.3.6). Although the snapshots from the MD simulation showed that PI leaves the catalytic site with the help of the residues 59−70, it can be hypothesized that PI could also be recruited to the active site of PimA with the active involvement of the residues 59−70. Our study also demonstrated that the binding of PI is comparatively less stable, which probably explains why any crystal structure of PI-bound PimA was not obtained despite several attempts.[18]

3.3.7.2. PimA-PIM. The interactions between PimA-PIM had not been studied much before. The product PIM showed interactions with the residues 59−70 of PimA throughout the simulation (Figures 9B and S7). MMGBSA analyses indicated strong interactions of P59, R68, and L69 with PIM (Section 3.3.4.2). In the active site, mannose transfer from GDPM makes PIM from PI, and then PIM is again probably transferred to the inner membrane or to PimB′. The residues 73−86 of PimA are known to interact with the membrane, and we can hypothesize that these residues may be critical for the exit of PIM from PimA. Figure 9B shows that residues 73−86 come in close contact with PIM frequently during MD simulation. The residues 73−86 of PimA form an amphipathic α-helix (Figure 2A), which had been implicated in interacting with the plasma membrane.[40] PimA lost its phospholipid-binding ability when the residues, ^{77}RKVKK^{81}, were mutated to ^{77}SSVSS^{81}.[40] The charged residues ^{77}RKVKK^{81} may interact with the polar inositol, mannose, and phosphate groups, whereas the other hydrophobic residues of the amphipathic α-helix interact with the acyl chains of PIM. Our analyses led to hypothesize that along with residues 59−70, residues 73−86 may also help PIM to be released from PimA.

3.3.7.3. PimA-PI-GDPM. To get a glimpse of the actual events at the active site before the mannosyl transfer, PimA was simulated with both the substrates GDPM and PI. Representative snapshots (Figure S8) and minimum distance analyses (Figure 9C) of this simulation show that GDPM and PI did not reside close to each other for a long time. Further inspection also revealed that PI and GDPM form two H-bonds around 5.71 and 7.28 ns. A detailed analysis of the snapshots obtained at 5.71 ns revealed that the C2 of the inositol moiety stays only 7 Å apart from the C1 atom of the mannose group of GDPM (Figure S9). PimA, a retaining glycosyltransferase, may possibly involve a double displacement mechanism, where one of the intermediates is a mannose-enzyme bond, which is further attacked by the inositol 2-OH. The other possible pathway may involve a transition state, where a negatively charged phosphate and a positively charged oxocarbenium ion are formed, which is further attacked by the incoming nucleophile 2-OH of the inositol moiety of PI. E274 has previously been hypothesized as one of the potential nucleophiles in the mannosyl transfer reaction. The distance between the E274 carboxyl group and the mannose group was 10.2 Å (Figure S9). However, the closest distance between the H118 side chain and one of the polar hydroxyl group mannose sugar was 3.7 Å, which leads us to hypothesize that H118 containing a neutrally charged side chain at this pH may stabilize the oxocarbenium intermediate, which is later attacked by the inositol-OH. However, we should keep in mind that these close snapshots do not guarantee that this is "the reaction pathway" actually followed before the mannose transfer reaction, and thus, these interpretations should be considered very carefully. Further investigation is required before a conclusion can be reached regarding the retaining mechanism of PimA.

Previous studies had already shown that the amphipathic α-helix formed by residues 73−86 are essential for membrane binding *in vitro* and *in vivo*.[40] The residues R77, K78, K80, and K81 are absolutely important for PimA activity.[40] In our MD simulation studies, we observed that the substrate PI, while present with GDPM, deviates from the active site and remains

https://doi.org/10.1021/acsomega.2c00832
ACS Omega 2022, 7, 19288−19304

stably bound near residues 73−86 (Figure S8), where these positively charged residues interact with the polar inositol group and the hydrophobic residues interact with the acyl chains. This is an important observation as it clearly shows that there could be a possible pathway where PI from the inner membrane of mycobacteria is probably recruited to PimA by residues 73−86 and then further it is carried to the active site by residues 59−70. Secondary structure transition analyses showed that the residues 59−70 tend to form β-sheet in the presence of PI. Section 3.3.7.1 showed that PI interacted with the residues for 130 ns before deviating from the active site. Even in the presence of GDPM, PI interacted with the residues 59−70 till ∼50 ns before drifting toward the α2-amphipathic helix. This shows that these residues may help PI transition from the membrane to the active site of PimA.

3.3.7.4. PimA-PIM-GDP. Acting alone on PimA, PIM interacted with the residues 59−70 throughout, as previously shown in Section 3.3.7.2. MMGBSA analyses showed strong interaction of PIM with the residues P59, R68, and L69 of PimA. Even with the presence of GDP, PIM interacted with the residues 59−70 frequently during the MD simulation (Figure 9D). PIM and GDP interact closely for a brief period of time (∼47−53 ns) and then deviate from each other (Figures 9D and S10−S11), similar to the association between PI and GDPM at the active site of PimA (Figure 9C). PIM slowly moved to the residues 73−86 from the active site between 270 and 290 ns (Figure 9D). It may be possible that the residues 73−86 may play important roles in delivering the product PIM to the inner membrane from the active site of PimA.

3.3.7.5. Hypothesized Mannosyl Transfer Scheme of PimA. Based on the findings of this study and the data from previous experiments, we propose a hypothetical model of mannosyltransferase activity of PimA (Figure 10). It had been previously shown that PI showed stronger binding to the PimA-GDP complex than PimA alone.[6] Previous SAXS data[42] and our MD analyses (Sections 3.3.1.2 and 3.3.2) indicate strongly that the PimA-GDP complex adopts a closed conformation. Together, this shows PI can possibly be recruited to the relatively closed conformation of PimA too. Our MMGBSA analyses indicated that GDPM will tend to bind first to PimA than PI (Table 2, Section 3.3.4.1). Thus, we may hypothesize that GDPM is recruited first (Figure 10A,B) and this binding promotes a relatively closed conformation of PimA, following which PI is recruited (Figure 10C). The interactions of GDPM and PimA also showed instances (Figure S10) where PimA adopts relatively open conformation. PI, a component of the inner membrane of mycobacteria, may first interact with the residues 73−86 of PimA (Figure 10C) and probably then be carried to the active site by the residues 59−70 (Figure 10D). Docking studies (Section 3.2), RMSF analyses (Section 3.3.3), and MMGBSA analyses (Section 3.3.4) indicated that residues Y9, R68, L69, R196, and R201 are possibly involved to bring the two substrates GDPM and PI closer to each other. A limitation of MD simulation is that it cannot account for the bond breaking or formation. Thus, although we observe GDPM and PI facing each other for a short time, we cannot conclude that this was indeed the mannose transfer pathway (Figure 10E). Once PIM and GDP are formed (Figure 10F), we observe that the products PIM and GDP also come into close contact for a brief period (Figure 9D), and then PIM is displaced. RMSD, R_g, PCA, and MMGBSA analyses showed that GDP-bound PimA adopts the most stable structure among all of the ligand-bound PimA. PIM is probably released first (Figure 10G), as indicated by the ΔG_{bind} and then GDP is released (Figure 10H) to prepare PimA to start for the next cycle of mannose transfer. Further studies are required to better understand the mechanism of mannose transfer by PimA.

4. CONCLUSIONS

In this study, we obtained the docked structures of PimA with PI and PIM, which showed that the residue R201, conserved in both PimA and PimB′, play important roles in binding both PI and PIM. The residues ^{8}PYS^{10}, P40, the loop formed by residues 59−70, residues ^{95}EXAP^{99}, and residues 124−131 may play important roles in the mannosyltransferase activity of PimA by interacting with the acyl chains of PI or PIM. Our MD simulation studies clearly showed that PimA can adopt two different conformations, *i.e.*, open and closed. MD trajectory analyses also showed that the binding of PI and PIM at the active site is not stable, and both these lipids show significant displacement during the simulation. RMSD, R_g, and PCA indicated that free PimA is most flexible, whereas the GDP-bound PimA is the least flexible when one ligand is bound to PimA. However, when both GDPM and PI are bound, PimA showed the least flexibility, indicating the mannosyl transfer reaction is probably facilitated by a closed conformation of PimA. RMSF analyses also suggested allosteric communication between the two domains of PimA upon binding with the ligands. MMGBSA analyses indicated that GDPM is probably recruited to PimA first, which is further stabilized by the incorporation of PI, as indicated by H-bond analyses. Our MD simulation analyses also indicated that the residues 59−70 play important roles in binding PI and PIM, and may possibly be involved in the recruitment of PI to the active site or in the release of PIM from the active site of PimA. The residues 73−86 of PimA interacted with PI in the presence of GDPM and thus hypothesized to be involved in recruiting PI from the inner membrane of mycobacteria. The residues Y9, P59, R68, L69, N97, R196, R201, K202, and R228 were shown to play important roles while interacting with the substrates or the products and thus are hypothesized to be critical for the mannosyltransferase activity of PimA.

■ ASSOCIATED CONTENT

Supporting Information

The Supporting Information is available free of charge at https://pubs.acs.org/doi/10.1021/acsomega.2c00832.

Figures S1−S12 and Tables S1−S2 (PDF)

The ligand parameter files for the MD simulations (ZIP)

■ AUTHOR INFORMATION

Corresponding Authors

Amit Ghosh − *School of Energy Science and Engineering and P.K. Sinha Centre for Bioenergy and Renewables, Indian Institute of Technology Kharagpur, Kharagpur 721302, India;* orcid.org/0000-0003-3514-885X; Email: amitghosh@iitkgp.ac.in

Amit Kumar Das − *Department of Biotechnology, Indian Institute of Technology Kharagpur, Kharagpur 721302, India;* orcid.org/0000-0001-9703-1898; Email: amitk@bt.iitkgp.ac.in

https://doi.org/10.1021/acsomega.2c00832
ACS Omega 2022, 7, 19288−19304

Author

Gourab Bhattacharje − *Department of Biotechnology, Indian Institute of Technology Kharagpur, Kharagpur 721302, India;* orcid.org/0000-0001-7823-8033

Complete contact information is available at: https://pubs.acs.org/10.1021/acsomega.2c00832

Author Contributions

G.B. contributed to conceptualization, investigation, methodology, software, data processing, visualization, and writing of the original draft. A.G. contributed to methodology. A.K.D. contributed to conceptualizing and funding acquisition of this project. Both A.G. and A.K.D. supervised the project and contributed to reviewing and editing the original draft.

Notes

The authors declare no competing financial interest.
Data and software are available upon request.

■ ACKNOWLEDGMENTS

G.B. is grateful to Indian Institute of Technology Kharagpur for providing an institute fellowship. The authors are also thankful to National Supercomputing Machine (NSM) for providing computing resources of "PARAM Shakti" at IIT Kharagpur, which is implemented by C-DAC and supported by the Ministry of Electronics and Information Technology (MeitY) and Department of Science and Technology (DST), Government of India. Department of Science and Technology and Biotechnology, Govt. of West Bengal, is acknowledged for financial assistance (811(Sanc.)/ST/P/S&T/2G-49/2018). Department of Biotechnology, Government of India, is also acknowledged for financial help (grant no. BT/PR40990/MED/29/1540/2020). A.G. thanks SERB-Department of Science and Technology-GoI (grant no. CRG/2020/002080), Department of Biotechnology-GoI (grant no. BT/RLF/Re-entry/06/2013), and Scheme for Promotion of Academic and Research Collaboration (SPARC), MHRD-GoI (grant no. SPARC/2018-2019/P265/SL).

■ ABBREVIATIONS

GDP:guanosine diphosphate
GDPM:guanosine diphosphate mannose
GT:glycosyl transferase
LM:lipomannan
LAM:lipoarabinomannan
PDB:Protein Data Bank
PI:phosphatidylinositol
PIM:phosphatidylinositol mannoside
PIM_2:phosphatidylinositol dimannoside
PIM_6:phosphatidylinositol hexamannoside
PimA:phosphatidylinositol mannosyltransferase A
PimB′:phosphatidylinositol mannosyltransferase B′
Man (M):mannose
MD:molecular dynamics
PCA:principal component analysis

■ REFERENCES

(1) Brennan, P. J.; Nikaido, H. The Envelope of Mycobacteria. *Annu. Rev. Biochem.* **1995**, *64*, 29−63.
(2) Ballou, C. E.; Vilkas, E.; Lederer, E. Structural studies on the myo-inositol phospholipids of *Mycobacterium tuberculosis* (var. bovis, strain BCG). *J. Biol. Chem.* **1963**, *238*, 69−76.
(3) Lee, Y. C.; Ballou, C. E. Structural Studies on the myo-inositol mannosides from the glycolipids of *Mycobacterium tuberculosis* and *Mycobacterium phlei*. *J. Biol. Chem.* **1964**, *239*, 1316−1327.
(4) Guerin, M. E.; Korduláková, J.; Alzari, P. M.; Brennan, P. J.; Jackson, M. Molecular basis of phosphatidyl-myo-inositol mannoside biosynthesis and regulation in Mycobacteria. *J. Biol. Chem.* **2010**, *285*, 33577−33583.
(5) Korduláková, J.; Gilleron, M.; Mikuová, K.; Puzo, G.; Brennan, P. J.; Gicquel, B.; Jackson, M. Definition of the first mannosylation step in phosphatidylinositol mannoside synthesis. *J. Biol. Chem.* **2002**, *277*, 31335−31344.
(6) Guerin, M. E.; Kordulakova, J.; Schaeffer, F.; Svetlikova, Z.; Buschiazzo, A.; Giganti, D.; Gicquel, B.; Mikusova, K.; Jackson, M.; Alzari, P. M. Molecular recognition and interfacial catalysis by the essential phosphatidylinositol mannosyltransferase PimA from mycobacteria. *J. Biol. Chem.* **2007**, *282*, 20705−20714.
(7) Batt, S. M.; Jabeen, T.; Mishra, A. K.; Veerapen, N.; Krumbach, K.; Eggeling, L.; Besra, G. S.; Fütterer, K. Acceptor substrate discrimination in phosphatidyl-myo-inositol mannoside synthesis: Structural and mutational analysis of mannosyltransferase *Corynebacterium glutamicum* PimB′. *J. Biol. Chem.* **2010**, *285*, 37741−37752.
(8) Boldrin, F.; Anso, I.; Alebouyeh, S.; Sevilla, I. A.; Geijo, M.; Garrido, J. M.; Marina, A.; Mazzabò, L. C.; Segafreddo, G.; Guerin, M. E.; Manganelli, R.; Prados-Rosales, R. The phosphatidyl- *myo* -inositol dimannoside acyltransferase PatA is essential for *Mycobacterium tuberculosis* growth *in vitro* and *in vivo*. *J. Bacteriol.* **2021**, *203*, e00439−20.
(9) Sancho-Vaello, E.; Albesa-Jové, D.; Rodrigo-Unzueta, A.; Guerin, M. E. Structural basis of phosphatidyl-myo-inositol mannosides biosynthesis in mycobacteria. *Biochim. Biophys. Acta, Mol. Cell Biol. Lipids* **2017**, *1862*, 1355−1367.
(10) Kremer, L.; Gurcha, S. S.; Bifani, P.; Hitchen, P. G.; Baulard, A.; Morris, H. R.; Dell, A.; Brennan, P. J.; Besra, G. S. Characterization of a putative α-mannosyltransferase involved in phosphatidylinositol trimannoside biosynthesis in *Mycobacterium tuberculosis*. *Biochem. J.* **2002**, *363*, 437−447.
(11) Morita, Y. S.; Patterson, J. H.; Billman-Jacobe, H.; McConville, M. J. Biosynthesis of mycobacterial phosphatidylinositol mannosides. *Biochem. J.* **2004**, *378*, 589−597.
(12) Eagen, W. J.; Baumoel, L. R.; Osman, S. H.; Rahlwes, K. C.; Morita, Y. S. Deletion of PimE mannosyltransferase results in increased copper sensitivity in *Mycobacterium smegmatis*. *FEMS Microbiol. Lett.* **2018**, *365*, No. fny025.
(13) Mishra, A. K.; Driessen, N. N.; Appelmelk, B. J.; Besra, G. S. Lipoarabinomannan and related glycoconjugates: Structure, biogenesis and role in *Mycobacterium tuberculosis* physiology and host-pathogen interaction. *FEMS Microbiol Rev.* **2011**, *35*, 1126−1157.
(14) Källenius, G.; Correia-Neves, M.; Buteme, H.; Hamasur, B.; Svenson, S. B. Lipoarabinomannan, and its related glycolipids, induce divergent and opposing immune responses to *Mycobacterium tuberculosis* depending on structural diversity and experimental variations. *Tuberculosis* **2016**, *96*, 120−130.
(15) Boldrin, F.; Ventura, M.; Degiacomi, G.; Ravishankar, S.; Sala, C.; Svetlikova, Z.; Ambady, A.; Dhar, N.; Kordulakova, J.; Zhang, M.; Serafini, A.; Vishwas, V. G.; Kolly, G. S.; Kumar, N.; Palu′, G.; Guerin, M. E.; Mikusova, K.; Cole, K. M.; Manganelli, R. The phosphatidyl-myo-inositol mannosyltransferase PimA is essential for *Mycobacterium tuberculosis* growth *in vitro* and *in vivo*. *J. Bacteriol.* **2014**, *196*, 3441−3451.
(16) Lairson, L. L.; Henrissat, B.; Davies, G. J.; Withers, S. G. Glycosyltransferases: structures, functions, and mechanisms. *Annu. Rev. Biochem.* **2008**, *77*, 521−555.
(17) Coutinho, P. M.; Deleury, E.; Davies, G. J.; Henrissat, B. An evolving hierarchical family classification for glycosyltransferases. *J. Mol. Biol.* **2003**, *328*, 307−317.
(18) Giganti, D.; Albesa-Jové, D.; Urresti, S.; Rodrigo-Unzueta, A.; Martínez, M. A.; Comino, N.; Barilone, N.; Bellinzoni, M.; Chenal, A.; Guerin, M. E.; Alzari, P. M. Secondary structure reshuffling modulates

glycosyltransferase function at the membrane. *Nat. Chem. Biol.* **2015**, *11*, 16−18.
(19) Rodrigo-Unzueta, A.; Martinez, M. A.; Comino, N.; Alzari, P. M.; Chenal, A.; Guerin, M. E. Molecular basis of membrane association by the phosphatidylinositol mannosyltransferase PimA enzyme from Mycobacteria. *J. Biol. Chem.* **2016**, *291*, 13955−13963.
(20) Rodrigo-Unzueta, A.; Ghirardello, M.; Urresti, S.; Delso, I.; Giganti, D.; Anso, I.; Trastoy, B.; Comino, N.; Tersa, M.; D'Angelo, C.; Cifuente, J. O.; Marina, A.; Liebau, J.; Mäler, L.; Chenal, A.; Albesa-Jové, D.; Merino, P.; Guerin, M. E. Dissecting the structural and chemical determinants of the "open-to-closed" motion in the mannosyltransferase PimA from mycobacteria. *Biochemistry* **2020**, *59*, 2934−2945.
(21) Bateman, A.; Martin, M. J.; Orchard, S.; Magrane, M.; Agivetova, R.; Ahmad, S.; Alpi, E.; Bowler-Barnett, E. H.; Britto, R.; Bursteinas, B.; Bye-A-Jee, H.; Coetzee, R.; Cukura, A.; da Silva, A.; Denny, P.; Dogan, T.; Ebenezer, T.; Fan, J.; Castro, L. G.; Garmiri, P.; Georghiou, G.; Gonzales, L.; Hatton-Ellis, E.; Hussein, A.; Ignatchenko, A.; Insana, G.; Ishtiaq, R.; Jokinen, P.; Joshi, V.; Jyothi, D.; Lock, A.; Lopez, R.; Luciani, A.; Luo, J.; Lussi, Y.; MacDougall, A.; Madeira, F.; Mahmoudy, M.; Menchi, M. A.; Mishra, M.; Moulang, K.; Nightingale, A.; Oliveira, C. S.; Pundir, S.; Qi, G.; Raj, S.; Rice, D.; Lopez, M. R.; Saidi, R.; Sampson, J.; Sawford, T.; Speretta, E.; Turner, E.; Tyagi, N.; Vasudev, P.; Volynkin, V.; Warner, K.; Watkins, X.; Zaru, R.; Zellner, H.; Bridge, A.; Poux, S.; Redaschi, N.; Aimo, L.; Argoud-Puy, G.; Auchincloss, A.; Axelsen, K.; Bansal, P.; Baratin, D.; Blatter, M. C.; Bolleman, J.; Boutet, E.; Breuza, L.; Casals-Casas, C.; de Castro, E.; Echioukh, K. C.; Coudert, E.; Cuche, B.; Doche, M.; Dornevil, D.; Estreicher, A.; Famiglietti, M. L.; Feuermann, M.; Gasteiger, E.; Gehant, S.; Gerritsen, V.; Gos, A.; Gruaz-Gumowski, N.; Hinz, U.; Hulo, C.; Hyka-Nouspikel, N.; Jungo, F.; Keller, G.; Kerhornou, A.; Lara, V.; le Mercier, P.; Lieberherr, D.; Lombardot, T.; Martin, X.; Masson, P.; Morgat, A.; Neto, T. B.; Paesano, S.; Pedruzzi, I.; Pilbout, S.; Pourcel, L.; Pozzato, M.; Pruess, M.; Rivoire, C.; Sigrist, C.; Sonesson, K.; Stutz, A.; Sundaram, S.; Tognolli, M.; Verbregue, L.; Wu, C. H.; Arighi, C. N.; Arminski, L.; Chen, C.; Chen, Y.; Garavelli, J. S.; Huang, H.; Laiho, K.; McGarvey, P.; Natale, D. A.; Ross, K.; Vinayaka, C. R.; Wang, Q.; Wang, Y.; Yeh, L. S.; Zhang, J.; Ruch, P.; Teodoro, D. UniProt: the universal protein knowledgebase in 2021. *Nucleic Acids Res.* **2021**, *49*, D480−D489.
(22) Madeira, F.; mi Park, Y.; Lee, J.; Buso, N.; Gur, T.; Madhusoodanan, N.; Basutkar, P.; Tivey, A. R. N.; Potter, S. C.; Finn, R. D.; Lopez, R. The EMBL-EBI search and sequence analysis tools APIs in 2019. *Nucleic Acids Res.* **2019**, *47*, W636−W641.
(23) Berman, H. M. The Protein Data Bank. *Nucleic Acids Res.* **2000**, *28*, 235−242.
(24) Robert, X.; Gouet, P. Deciphering key features in protein structures with the new ENDscript server. *Nucleic Acids Res.* **2014**, *42*, W320−W324.
(25) Mallevaey, T.; Clarke, A. J.; Scott-Browne, J. P.; Young, M. H.; Roisman, L. C.; Pellicci, D. G.; Patel, O.; Vivian, J. P.; Matsuda, J. L.; McCluskey, J.; Godfrey, D. I.; Marrack, P.; Rossjohn, J.; Gapin, L. A molecular basis for NKT cell recognition of CD1d-self-antigen. *Immunity* **2011**, *34*, 315−326.
(26) Zajonc, D. M.; Ainge, G. D.; Painter, G. F.; Severn, W. B.; Wilson, I. A. Structural Characterization of Mycobacterial Phosphatidylinositol Mannoside Binding to Mouse CD1d. *J. Immunol.* **2006**, *177*, 4577−4583.
(27) Hanwell, M. D.; Curtis, D. E.; Lonie, D. C.; Vandermeersch, T.; Zurek, E.; Hutchison, G. R. Avogadro: an advanced semantic chemical editor, visualization, and analysis platform. *J. Cheminform.* **2012**, *4*, No. 17.
(28) Schüttelkopf, A. W.; van Aalten, D. M. F. *PRODRG*: a tool for high-throughput crystallography of protein−ligand complexes. *Acta Crystallogr., Sect. D: Biol. Crystallogr.* **2004**, *60*, 1355−1363.
(29) Olsson, M. H. M.; Søndergaard, C. R.; Rostkowski, M.; Jensen, J. H. PROPKA3: Consistent Treatment of Internal and Surface Residues in Empirical p K_a Predictions. *J. Chem. Theory Comput.* **2011**, *7*, 525−537.
(30) Grosdidier, A.; Zoete, V.; Michielin, O. SwissDock, a protein-small molecule docking web service based on EADock DSS. *Nucleic Acids Res.* **2011**, *39*, W270−W277.
(31) Pettersen, E. F.; Goddard, T. D.; Huang, C. C.; Couch, G. S.; Greenblatt, D. M.; Meng, E. C.; Ferrin, T. E. UCSF Chimera: a visualization system for exploratory research and analysis. *J. Comput. Chem.* **2004**, *25*, 1605−1612.
(32) Abraham, M. J.; Murtola, T.; Schulz, R.; Páll, S.; Smith, J. C.; Hess, B.; Lindah, E. Gromacs: High performance molecular simulations through multi-level parallelism from laptops to supercomputers. *SoftwareX* **2015**, *1−2*, 19−25.
(33) Waterhouse, A.; Bertoni, M.; Bienert, S.; Studer, G.; Tauriello, G.; Gumienny, R.; Heer, F. T.; de Beer, T. A. P.; Rempfer, C.; Bordoli, L.; Lepore, R.; Schwede, T. SWISS-MODEL: homology modelling of protein structures and complexes. *Nucleic Acids Res.* **2018**, *46*, W296−W303.
(34) Vanommeslaeghe, K.; Hatcher, E.; Acharya, C.; Kundu, S.; Zhong, S.; Shim, J.; Darian, E.; Guvench, O.; Lopes, P.; Vorobyov, I.; Mackerell, A. D. CHARMM general force field: A force field for drug-like molecules compatible with the CHARMM all-atom additive biological force fields. *J. Comput. Chem.* **2010**, *31*, 671−690.
(35) Martínez, L.; Andrade, R.; Birgin, E. G.; Martínez, J. M. PACKMOL: A package for building initial configurations for molecular dynamics simulations. *J. Comput. Chem.* **2009**, *30*, 2157−2164.
(36) Adcock, S. A.; McCammon, J. A. Molecular Dynamics: Survey of methods for simulating the activity of proteins. *Chem. Rev.* **2006**, *106*, 1589−1615.
(37) Schrödinger, L.; DeLano, W.*PyMOL*, 2020.
(38) Miller, B. R.; McGee, T. D.; Swails, J. M.; Homeyer, N.; Gohlke, H.; Roitberg, A. E. *MMPBSA.py*: An efficient program for end-state free energy calculations. *J. Chem. Theory Comput.* **2012**, *8*, 3314−3321.
(39) Valdés-Tresanco, M. S.; Valdés-Tresanco, M. E.; Valiente, P. A.; Moreno, E. gmx_MMPBSA: A new tool to perform end-state free energy calculations with GROMACS. *J. Chem. Theory Comput.* **2021**, *17*, 6281−6291.
(40) Guerin, M. E.; Schaeffer, F.; Chaffotte, A.; Gest, P.; Giganti, D.; Korduláková, J.; van der Woerd, M.; Jackson, M.; Alzari, P. M. Substrate-induced conformational changes in the essential peripheral membrane-associated mannosyltransferase PimA from mycobacteria. Implications for catalysis. *J. Biol. Chem.* **2009**, *284*, 21613−21625.
(41) Albesa-Jové, D.; Giganti, D.; Jackson, M.; Alzari, P. M.; Guerin, M. E. Structure-function relationships of membrane-associated GT-B glycosyltransferases. *Glycobiology* **2014**, *24*, 108−124.
(42) Giganti, D.; Alegre-Cebollada, J.; Urresti, S.; Albesa-Jové, D.; Rodrigo-Unzueta, A.; Comino, N.; Kachala, M.; López-Fernández, S.; Svergun, D. I.; Fernández, J. M.; Guerin, M. E. Conformational plasticity of the essential membrane-associated mannosyltransferase PimA from mycobacteria. *J. Biol. Chem.* **2013**, *288*, 29797−29808.
(43) Hu, Y.; Chen, L.; Ha, S.; Gross, B.; Falcone, B.; Walker, D.; Mokhtarzadeh, M.; Walker, S. Crystal structure of the MurG:UDP-GlcNAc complex reveals common structural principles of a superfamily of glycosyltransferases. *Proc. Natl. Acad. Sci. U.S.A.* **2003**, *100*, 845−849.
(44) Buschiazzo, A.; Ugalde, J. E.; Guerin, M. E.; Shepard, W.; Ugalde, R. A.; Alzari, P. M. Crystal structure of glycogen synthase: homologous enzymes catalyze glycogen synthesis and degradation. *EMBO J.* **2004**, *23*, 3196−3205.
(45) Sheng, F.; Jia, X.; Yep, A.; Preiss, J.; Geiger, J. H. The Crystal Structures of the Open and Catalytically Competent Closed Conformation of *Escherichia coli* Glycogen Synthase. *J. Biol. Chem.* **2009**, *284*, 17796−17807.
(46) Vetting, M. W.; Frantom, P. A.; Blanchard, J. S. Structural and Enzymatic Analysis of MshA from *Corynebacterium glutamicum*. *J. Biol. Chem.* **2008**, *283*, 15834−15844.
(47) Agarwal, P. K. Role of Protein Dynamics in Reaction Rate Enhancement by Enzymes. *J. Am. Chem. Soc.* **2005**, *127*, 15248−15256.

https://doi.org/10.1021/acsomega.2c00832
ACS Omega 2022, 7, 19288−19304